ELSEVIER

Marine and Petroleum Geology 15 (1998) 549–573

Marine and Petroleum Geology

The use of dipmeter data to constrain the structural geology of the Gullfaks Field, northern North Sea

J. Hesthammer[a,*], H. Fossen[b]

[a] *Statoil, GF/PETEK-GEO, N-5020 Bergen, Norway*
[b] *Department of Geology, University of Bergen, Allegt. 41, N-5007 Bergen, Norway*

Received 22 September 1997; revised 20 April 1998; accepted 25 April 1998

Abstract

Analyses of 23 km of dipmeter data from 48 wells on the Gullfaks Field, northern North Sea, have helped to constrain and understand the structural geology of the area. The analyses have verified the general structure obtained by seismic interpretation; i.e. a main, western domino system of rotated fault blocks and non-planar bedding and an eastern horst complex, separated by a collapsed anticline structure. In addition, subseismic structures have been revealed by the integrated use of dipmeter data, well log correlation, seismic data and core data.

Within the domino system, dip of bedding decreases towards the main faults to the west (large-scale drag). The effect of such large-scale drag decreases with depth, probably due to a vertical increase in consolidation and mechanical strength at the time of deformation. Within the accommodation zone, a modified fold structure is seen, whereas strata within the horst complex are generally subhorizontal.

More than half of all faults on the Gullfaks Field have developed a zone of local drag. Generally, only the northerly-trending faults are associated with drag. The interval affected by drag is typically some tens of meters wide, and is consistently wider in the hanging wall than the footwall. Due to the effect of drag, total offset may be up to one order of magnitude larger than the amount of missing section identified from well log correlation. There is no apparent relationship between interval affected by drag and lithology. However, drag is less abundant in more consolidated rocks at deeper stratigraphic levels.

Minor faults are less abundant than expected from a power-law down-scaling of seismically detectable faults, and are not particularly common within the large-scale drag zones. It is suggested that a significant amount of subseismic deformation occurs on a scale below resolution of dipmeter data, probably by 'ductile' flow rather than discrete faulting. North-trending minor faults are most common and will restrict fluid flow in an E–W direction due to cataclasis and phyllosilicate smear associated with abundant deformation bands (micro-faults).

Keywords: Structural geology; Dipmeter data; Gullfaks Field

1. Introduction

As many new oil and gas fields and remaining well targets in producing fields are economically marginal, the need for a sound understanding of the structural geology in such areas increases. Integrated use of different types of data is necessary to achieve this goal. In field development, this involves both seismic, production and various types of well data. In structurally complex areas, seismic data are typically of poor quality, and production data may be difficult to interpret. In such cases, it is important to utilise available well information such as dipmeter data, which is the theme of the present article. Dipmeter data reflect dip and azimuth of bedding (Schlumberger, 1986; Serra, 1989; Schlumberger, 1990; 1991). Variations of these parameters along the bore holes help improve our understanding of the structural geology in faulted reservoirs (Bengtson, 1981; Schlumberger, 1986; Etchecopar and Bonnetain, 1989; Bigelow, 1993; Goetz, 1994).

The present study focuses on how the analyses of 23 km of dipmeter data from the structurally complex Gullfaks Field in the northern North Sea have helped to outline the structural characteristics of the field. We believe that the large amount of data available makes the Gullfaks Field particularly well suited for this type of study, and may serve as a guide for similar analyses on other fields. In the following, description and discussion of the results are provided.

* Corresponding author. Tel.: +47 55992130; fax: +47 55992097; e-mail: jonhe@statoil.no

S0264–8172/98/$—see front matter
PII: S0264–8172(98)00028–2

2. Structural setting

The Gullfaks Field is situated in block 34/10 in the western flank of the Viking Graben in the northern North Sea, south of the Snorre Field and southeast of the Statfjord Field (Fig. 1). The field covers an area of ca 55 km^2 and is developed from three platforms under the Norwegian license group consisting of Statoil (operator), Norsk Hydro and Saga Petroleum. Total recoverable reserves amount to ca. 310 mill. Sm^3 of oil and some 30 bill. Sm^3 of gas, and are produced from the Middle Jurassic Brent Group and the Lower Jurassic Cook and Statfjord Formations (Fig. 2).

The Gullfaks Field occupies the eastern half of a major (10–25 km wide) NNE–SSW trending fault block (the Gullfaks fault block; Fossen et al. in press) which is bounded by faults with km-scale displacement to the east and west. The major fault to the west separates the Gullfaks block from the giant fault block containing the Statfjord and Brent oil fields, whereas the bounding fault to the east borders the deeper parts of the Viking Graben.

At least two major rift phases have affected the area (e.g. Ziegler, 1982; Beach et al., 1987; Giltner, 1987; Badley et al., 1988; Thorne and Watts, 1989; Gabrielsen et al., 1990; Roberts et al., 1990; Færseth et al., 1995). The first rift phase is defined as a Permo-Triassic phase that affected the total width of the northern North Sea (Roberts et al., 1995; Færseth, 1996). The second rift event is termed the late Jurassic phase (e.g. Badley et al., 1988), and is more localised to the central portions of the northern North Sea (Viking and Sogn Grabens). Whereas the Permo-Triassic phase is at least as significant as the late Jurassic phase, late Jurassic deformation is more obvious on commercial seismic lines. Furthermore, because the majority of wells in the North Sea are confined to the Jurassic and younger section, the late Jurassic phase is best known from well data. The present study is mainly concerned with data from the Jurassic layers in the Gullfaks Field, and thus with the late Jurassic rift phase.

3. Geology of the Gullfaks Field

3.1. Stratigraphy

The deepest well on the Gullfaks Field (34/10-13) was drilled to ca 3350 m depth and penetrated 1340 m of Triassic sands and shales of the Hegre Group. The Scytian-Rhaetian Hegre Group (Fig. 2) comprises interbedded sandstones, claystones and shales deposited in a continental environment. Overlying this sequence are alluvial sandstones of the Rhaetian-Sinemurian Statfjord Formation. The Sinemurian-Toarcian Dunlin Group comprises marine clay- and siltstones of the Amundsen and Burton Formations, regressive, marine, silty claystones, muddy sandstones, and sands of the Cook Formation, and marine shales and siltstones of the Drake Formation. The mainly Bajocian-Early Bathonian Brent Group forms the upper and main part of the reservoir. The group is subdivided into the Broom, Rannoch, Etive, Ness, and Tarbert Formations deposited in a deltaic environment. A broad lithological subdivision can be made between the shaly Ness Formation and the sandy intervals below and above.

A time gap of up to 100 My is represented by the base Cretaceous (late Cimmerian) unconformity on the Gullfaks Field. This discontinuity separates Triassic and Jurassic sediments from Upper Cretaceous sediments and post-dates the major part of the faulting history of the Gullfaks Field. Up to 100 m of shales of the Upper Jurassic Heather Formation are locally preserved in the hanging walls to the main N–S trending faults, particularly in the western part of the field.

3.2. Structural outline

A general description and discussion of the structural geology of the Gullfaks Field is given in Fossen and Hesthammer (1998), and only the main points will be repeated here. Based on seismic interpretation and supported by dipmeter data (as described in this work), the Gullfaks Field can be divided into three contrasting compartments (Fig. 1); a western domino system with domino-style fault block geometry, a deeply eroded eastern horst complex of elevated subhorizontal layers and steep faults, and a transitional accommodation zone or collapsed fold structure.

The *domino system*, which constitutes the main and western part of the Gullfaks Field, is characterised by N–S trending faults (hereafter referred to as main faults) with displacements in the order of 50–500 m. The faults dip 25–30° to the east, whereas the strata within the fault blocks dip shallowly (typically 15°) to the west. These main faults typically show increasing complexity (bifurcation) towards higher reservoir levels.

The domino fault blocks are compartmentalised by several minor faults with throws less than 50 m. These faults have much more variable trends than the main faults. N–S striking, east-dipping minor faults generally have slightly steeper dips than the main faults when situated in the hanging wall, and slightly lower dips if they are located in a footwall position (footwall collapse structures). Minor faults striking in an E–W direction typically have steeper dips (45–90°) and are believed related to internal block deformation during differential slip along the main faults. NW–SE and NE–SW striking minor faults have variable throws and intermediate dips. Minor faults oriented antithetically to the main faults are less common and have variable, but mostly N–S strike. Core analyses typically indicate a relatively narrow 'damage

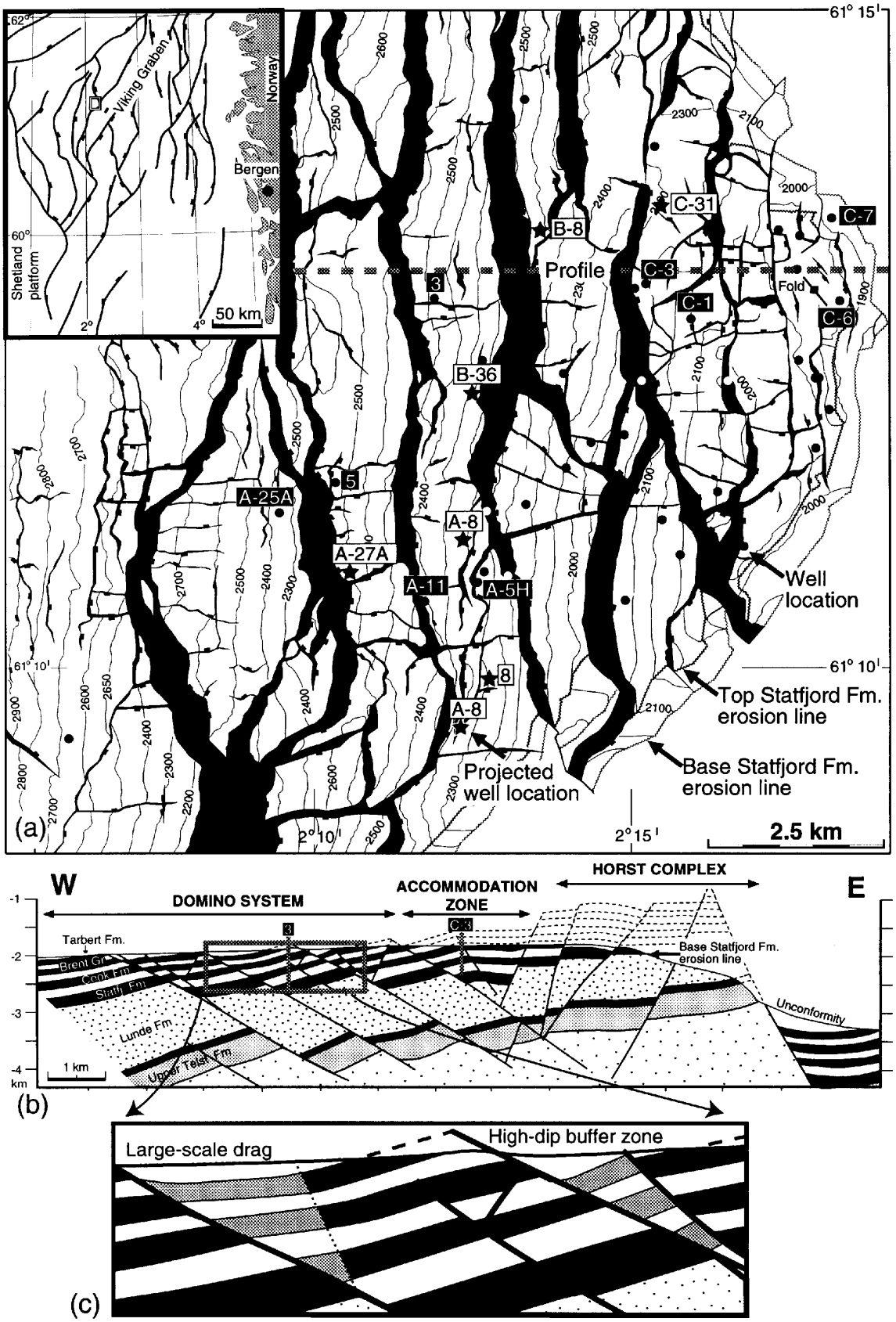

Fig. 1. (a) Structure map of the Statfjord Formation on the Gullfaks Field. Well locations indicated by a star are projected down from shallower reservoir levels. (b) E–W profile through the field showing the three structural domains. (c) The triangular drag zone and high dip buffer zone within the domino system. Inset map shows the location of the Gullfaks Field.

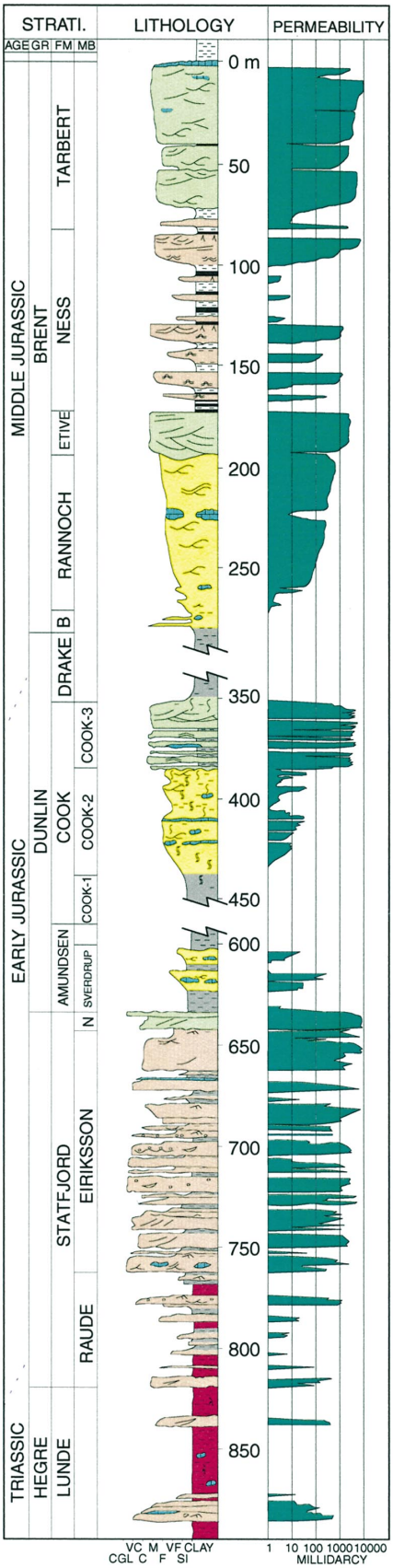

Fig. 2. Stratigraphic column for the Jurassic and Triassic reservoir units in the Gullfaks Field (modified from Tollefsen et al., 1994).

zone' (usually a few meters or less) associated with both minor and main faults.

The average dip of bedding in the domino area varies from 13° for the Brent Group to 16.6° for the deeper Statfjord Formation (calculated from depth-converted seismic interpretation). In addition, there is a general decrease in dip from the east (footwall position) to the west (hanging wall position) within the domino fault blocks. This change in dip gives rise to a gentle hanging-wall syncline, and is hereafter referred to as large-scale drag. The effect of this large-scale drag is greatest at shallower reservoir levels. Main faults in the *horst complex* are generally much steeper and more planar than those in the domino area, with dips of 60–70° being common. Both east- and west-dipping faults occur with a constant N–S strike.

The horst complex is characterised by poorer seismic data quality, which complicates mapping of minor faults. Seismically mappable minor faults are relatively steep (45–70°) and run subparallel to the main faults. Bedding within the horst complex is sub-horizontal or shallowly west-dipping. The *accommodation zone* is a graben structure which accommodates the different structural styles between the domino area and the horst complex. The zone is typically defined by a collapsed anticline with a west-dipping (ca 15°) western limb and a subhorizontal to gently east-dipping eastern limb. The fold axis plunges very gently to the NNW, and the opening angle is approximately 160° with a steeply dipping axial plane.

The accommodation zone is bounded by steep (65°) faults to the east and lower-angle (25–30°) faults to the west. Minor faults strike mostly N–S or E–W and have variable dip. Physical modelling (Fossen and Gabrielsen, 1996) and well data indicate that the accommodation zone is a complex area with many minor faults of which we have been able to identify only a small fraction.

4. Data

Several 3D reflection seismic surveys have been collected in the Gullfaks area. The current seismic interpretation is based on a 1985 acquisition which consists of some 10.000 km of seismic lines covering an area of ca 19 km in E–W direction and ca 14 km in N–S direction. The oil-bearing part of the structure covers an area of ca 55 km^2. More than 170 wells have been drilled on the Gullfaks Field since block 34/10 was awarded to the license group in 1978, yielding over 112 km of well section within the reservoir (Table 1).

Dipmeter data from a total of 23 km well section collected from 48 wells on the Gullfaks Field have been analysed with respect to structural dip of bedding. The instruments used on the Gullfaks Field for providing the information are Schlumberger's HDT, SHDT, FMS, and OBDT (for detailed description of the tools, see Schlumberger, 1986; Serra, 1989; Schlumberger, 1991).

Table 1
Amount of well data and dipmeter data available for interpretation. Simple trigonometric expressions were used to calculate the amount of available data projected into E–W and N–S direction. The nearly equal amount of data in these two directions suggests that there are no preferred orientations of drilling on the Gullfaks Field. It is important to be aware that, when dividing the number of faults observed from well log correlation and dipmeter data by the projected amount of well data in any direction, a too high number will result (simply because the projected amount of well data will always be less than the total amount).

Formation	% of drilled resevoir	Meters penetrated	Meters penetrated E–W	Meters penetrated N–S	m analysed dipmeter data	m analysed dipmeter data E–W	m analysed dipmeter data N–S
Heather	5.4	6,122	2,755	4,140	215	62	93
Tarbert	13.1	14,781	7,724	8,601	2,126	710	971
Ness	14.3	16,112	8,793	8,138	3,209	1,249	1,283
Etive	3.4	3.869	2,108	1,768	801	274	288
Rannoch	12.3	13,917	6,592	7,256	2,695	1,087	995
Broom	1.3	1,355	583	585	174	77	71
Drake	10.6	11,954	5,700	4,996	2,163	774	742
Cook	15.5	17,482	7,450	7,721	3,635	926	925
Burton	0.5	464	182	97	34	12	14
Amundsen	8.8	9,881	4,247	3,087	2,551	565	558
Statfjord	7.1	7,867	3,362	2,228	2,353	617	362
Hegre Group	7.7	8,719	4,318	2,982	2,708	598	401
All formations	100	112,523	53,814	51,599	22,664	6,951	6,703

In order to take full advantage of the information provided by the dipmeter tool, the resistivity curves must be processed to yield information on either structural or sedimentary bedding patterns. The processing methods used in this study are developed by Schlumberger (Schlumberger, 1986; 1990) and include the CLUSTER, MSD, OBDIP and FMS IMAGE processing methods.

The quality of the dipmeter data varies with the hole conditions, temperature and depth, type of mud used, rock type and tools. Generally, FMS data are of better quality than SHDT data due to the increased button density and borehole coverage. Similarly, SHDT gives better results than HDT due to improvements of the tool and the algorithms used in processing. Data from the OBDT are generally of poorer quality than any of the resistivity tools (related to the use of oil based mud), and results must accordingly be treated with care.

5. Large-scale structures

Forward modelling of the Gullfaks Field (Fossen and Hesthammer, 1998) suggests that the accommodation zone underwent considerably more internal deformation than both the horst complex and the domino system. The geometries within the horst complex require no internal (sub-seismic) deformation, whereas the domino system can be explained by a combination of ca 30° tilting and an average shear strain (γ) of 0.4 with the shear plane oriented synthetic to the main faults. This model implies an extension in the order of 80%, i.e. considerably more than the ca 40–50% indicated by a rigid block model (Rouby et al., 1996).

In general, there is good agreement between dipmeter data and seismic data, and the characteristic orientation of bedding in the domino system (westerly tilted layers), the horst complex (subhorizontal layering), and the accommodation zone (collapsed anticline structure) are reflected both in seismic (Fig. 3) and dipmeter data (Figs 4–5). Figure 4 displays stereonet plots from the three wells shown in Fig. 3. Both sets of data show west-dipping strata in the domino system as seen in well 34/10-3 which penetrates one of the rotated fault blocks. The anticline structure in the accommodation zone is verified by dipmeter data from well 34/10-C-1. The eastern fold limb shows very shallow dips to the east, whereas the western limb shows somewhat steeper dips to the west (C-1 in Fig. 4). Dip of strata in the hinge zone is subhorizontal. Dipmeter data from well 34/10-C-7, which is located in the horst complex, indicate subhorizontal strata in this area.

Figure 5 shows changes in dip and dip direction with respect to depth from the three wells. Dipmeter data from well 34/10-3 (Fig. 5a, domino system) show that the strata dip in a westerly direction with the amount of dip decreasing with depth. Although the same type of plot for well 34/10-C-1 (Fig. 5b, accommodation zone) shows much scatter (due to use of oil based mud; Stuart-Bruges, 1984; Dumont et al., 1987; Goetz, 1988), it can be seen that the dip of strata changes from an easterly direction above 2300 mMD (metres measured depth) to westerly dip below 2400 mMD. This example demonstrates that although dipmeter measurements from tools used in oil based mud are more scattered than those from water based mud, reliable structural dip and useful information

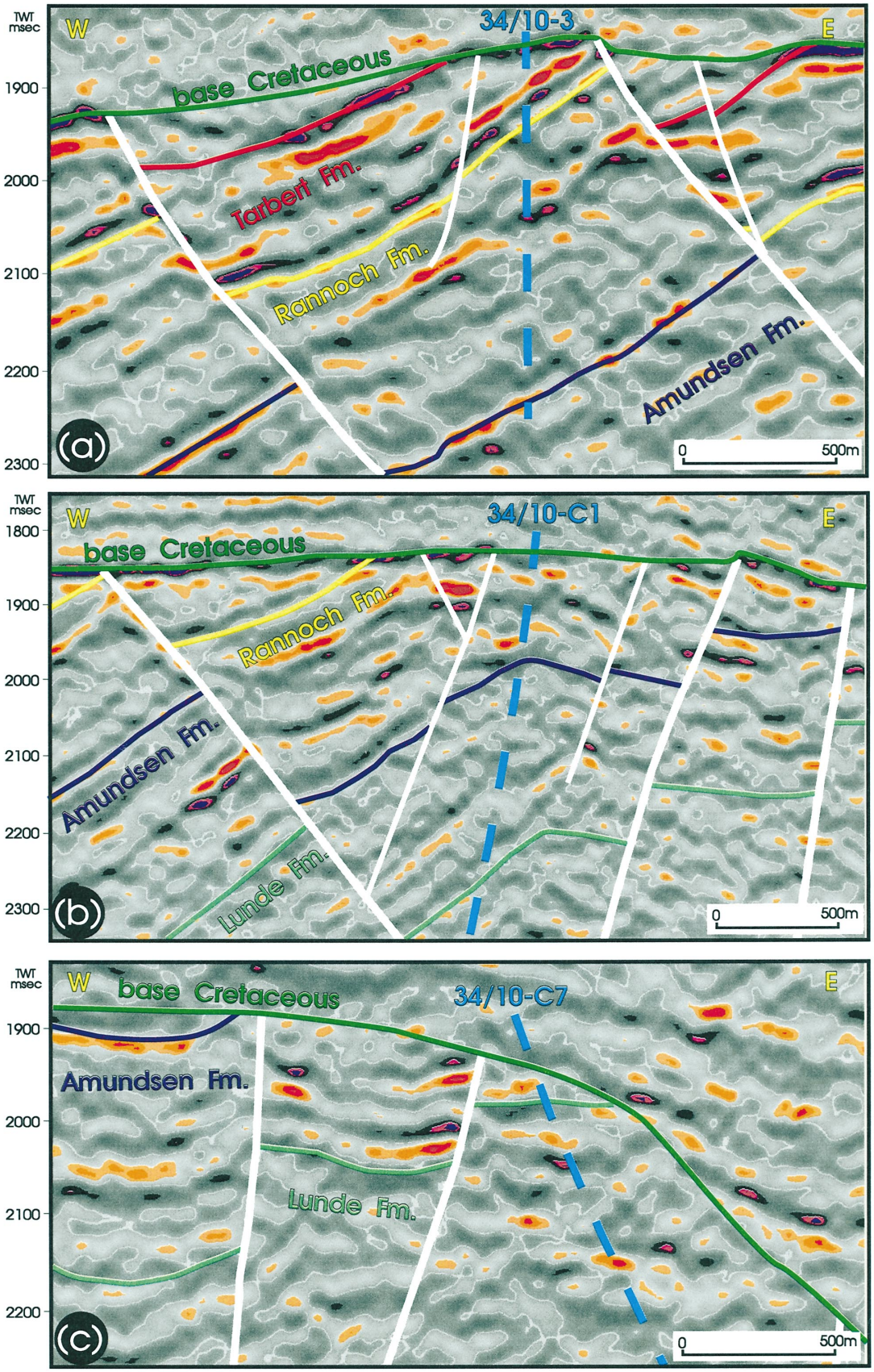

Fig. 3. Seismic profiles through (a) well 34/10-3 within the domino system, (b) well 34/10-C-1 from the accommodation zone, and (c) well 34/10-C-7 located within the horst complex. See Fig. 1 for location.

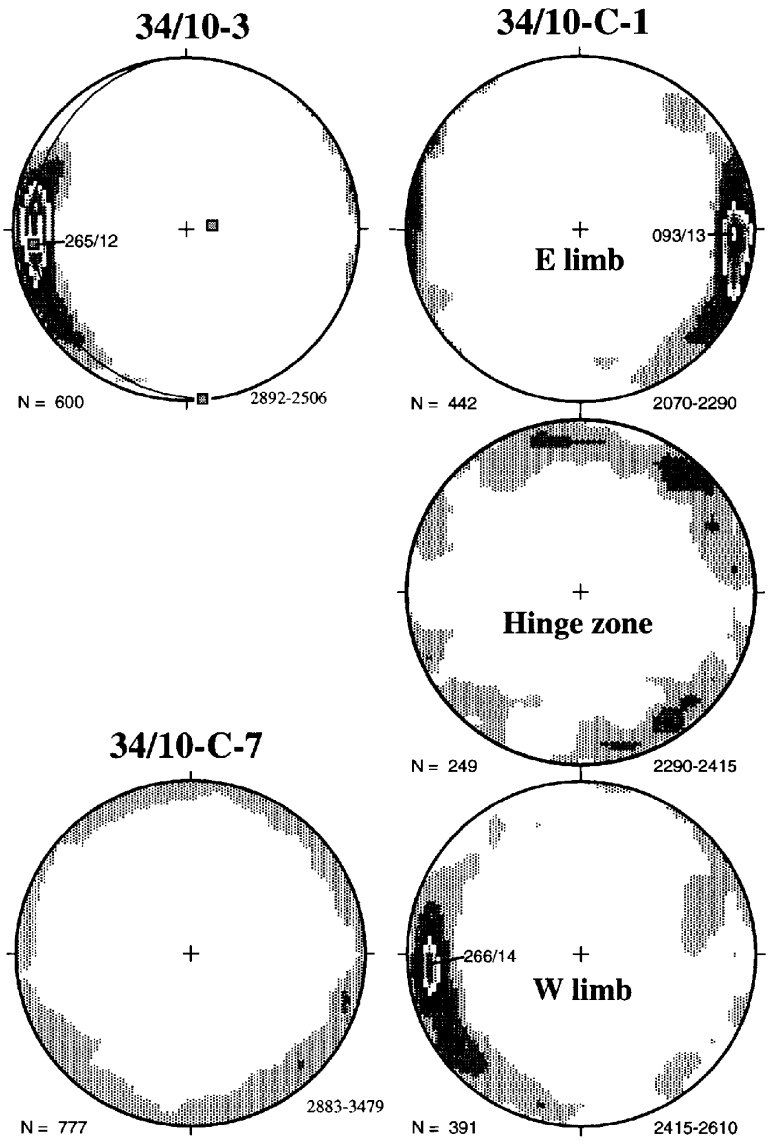

Fig. 4. Stereonet plots of dipmeter data (dip direction/dip) from the wells displayed in Fig. 3. See text for discussion. Depth interval indicated in lower right-hand corner (measured depth in well). Strata penetrated by well 34/10-C-1 : *eastern limb* : Cook and Amundsen Formations ; *hinge zone* : lower part of the Amundsen Formation and upper part of the Statfjord Formation ; *western limb* : lower part of the Statfjord Formation and upper part of the Lunde Formation.

can be achieved (see also Dumont et al., 1987). The zone from 2300–2400 mMD represents the hinge zone seen in Fig. 4. Strata in well 34/10-C-7 display shallow dips at all depths (Fig. 5c, horst complex), and as a result, the dip direction vs. depth plot shows much scatter.

5.1. Domino system

Figure 5(a) showed that amount of dip in well 34/10-3 decreases with depth. This change is consistent with the gradual decrease in dip towards the hanging wall side of the domino blocks which can be seen from the seismic data (Figs 3(a) and 6). The change in dip is most pronounced at shallower depths. A profile through the vertical exploration well 34/10-8 (Fig. 7), illustrates that the change in dip is most pronounced within a triangular area in the hanging wall part of the fault blocks, and that the decrease in dip occurs both to the west and with depth. Dipmeter data from the well verify this change in dip (Fig. 8). The dip vs depth plot (Fig. 9) shows that, just below the base Cretaceous unconformity, the dip is relatively high (around 19°), but decreases to subhorizontal at 2100 mMD. Strata in this interval dip to the west. Below 2100 mMD, dip increases with depth but dip direction changes to southeast. This pattern is characteristic of a fold structure with a subhorizontal fold axis (i.e. a non-plunging or shallowly plunging fold). The dip of strata increases to approximately 25° at 2180

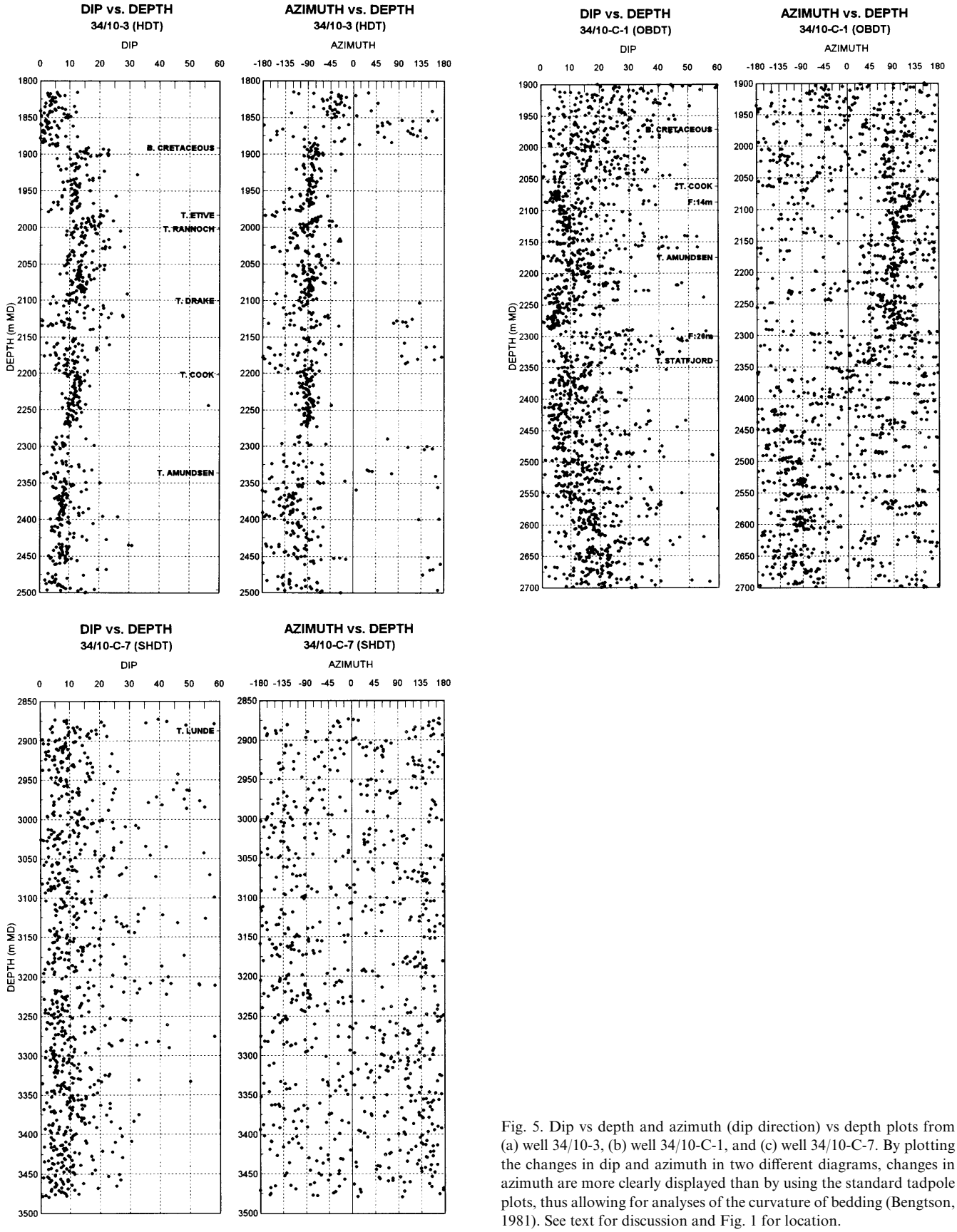

Fig. 5. Dip vs depth and azimuth (dip direction) vs depth plots from (a) well 34/10-3, (b) well 34/10-C-1, and (c) well 34/10-C-7. By plotting the changes in dip and azimuth in two different diagrams, changes in azimuth are more clearly displayed than by using the standard tadpole plots, thus allowing for analyses of the curvature of bedding (Bengtson, 1981). See text for discussion and Fig. 1 for location.

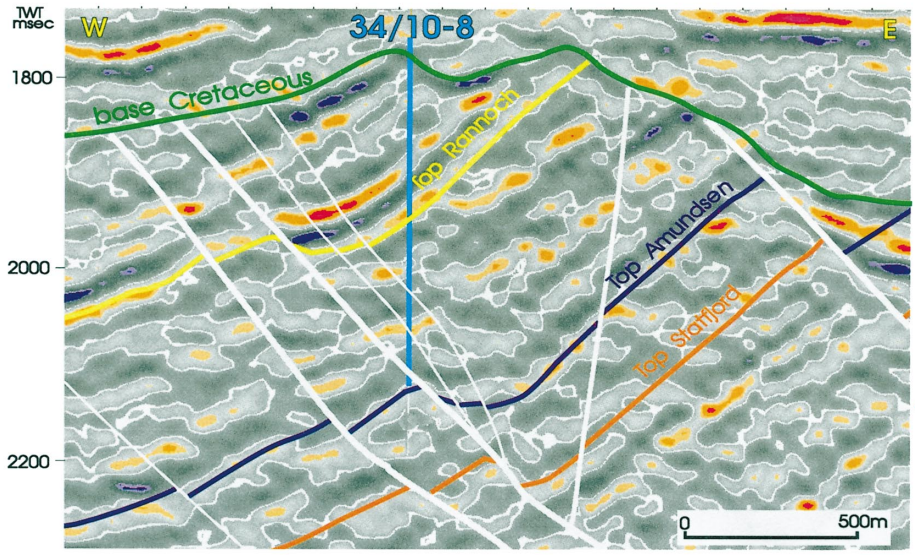

Fig. 6. Seismic line through well 34/10-8. Curved bedding traces appear in the hanging wall to the main fault and may in part be described as large-scale drag confined to a triangular zone. See Fig. 1 for location.

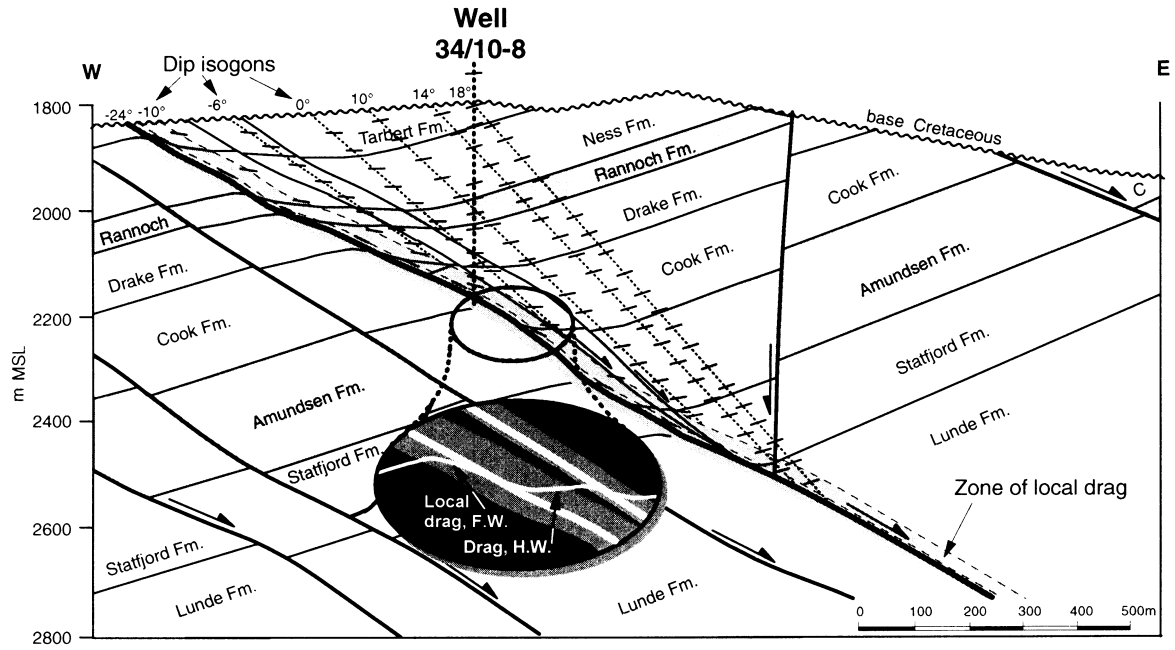

Fig. 7. Profile through well 34/10-8 based on seismic data and dipmeter data. Strata are dragged towards the main fault in a hanging wall position. Note how displacement at shallower levels are much less than at deeper levels. This large-scale drag (km-scale) defines a triangular zone and must be distinguished from local drag which affects the strata only some tens of meters away from the fault (see inset figure; the thin white line illustrates the changes in dip caused by local drag).

mMD where a fault with 14 m missing section intersects the well. Below this fault, data are not reliable enough for any confident interpretation. Since the well approaches the hanging wall side of the rotated domino fault block with depth, the decrease in dip with depth therefore reflects both lateral and vertical changes. The lateral decrease in dip towards the hanging wall part of the domino blocks is also seen from Fig. 10, where the average dip from the Rannoch, Amundsen and Statfjord Formations is plotted against distance to the next main fault to the east.

The large-scale drag within the triangle zone in a hanging wall position to the main faults is most easily explained by internal shear synthetic to, and steeper than the main faults (Fig. 11). In this model, shear strain increases towards the hanging wall side of the rotated fault blocks.

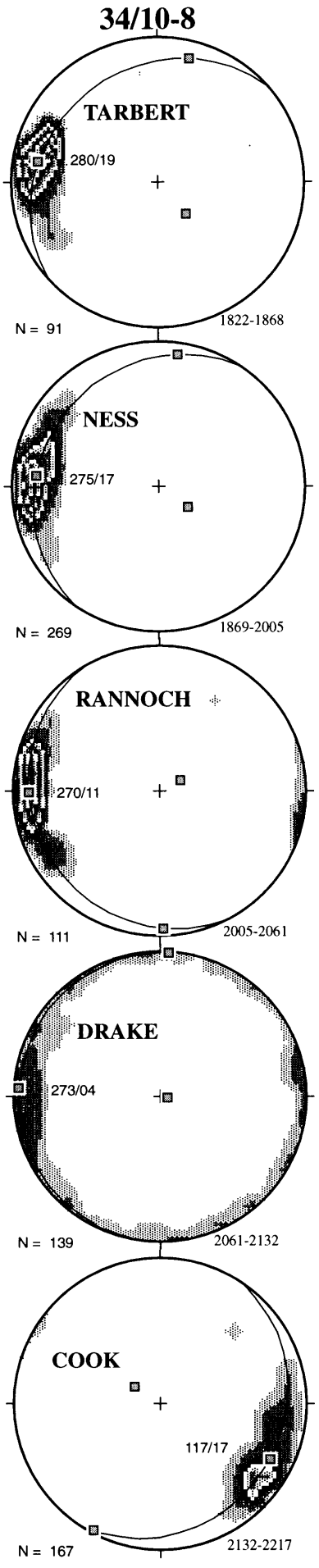

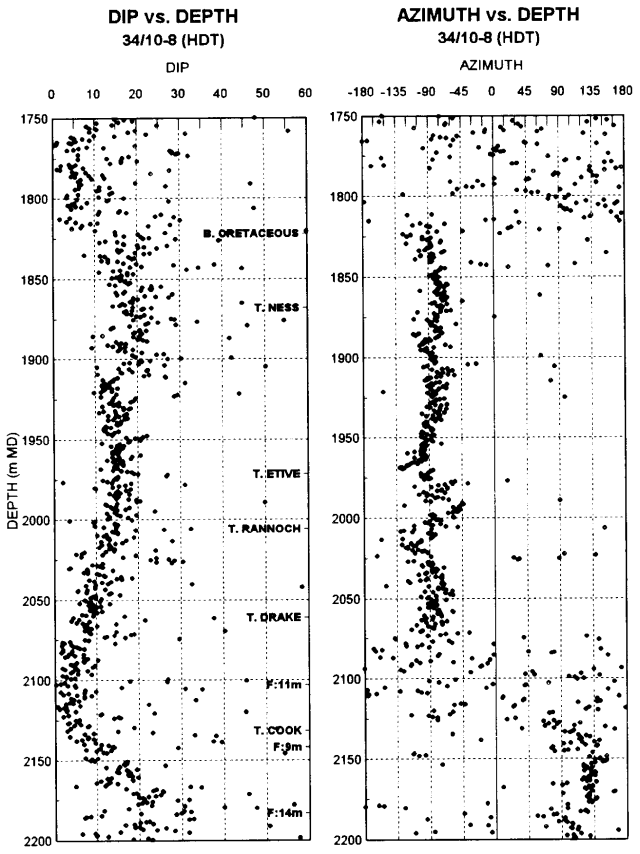

Fig. 9. The dip vs depth and dip direction vs depth plots from well 34/10-8 show an example of flattening drag (Bengtson, 1981) towards a main fault. Bedding is dragged from westerly dip at shallower reservoir levels to easterly dip at the base. The well does not penetrate the main fault, although several minor faults are encountered. See text for further discussion and Fig. 1 for location.

The model implies that the hanging walls to the rotated fault blocks are more deformed than the footwalls. Other examples where hanging walls are more deformed than footwalls are common both offshore (e.g. well 30/3-7S near the Veslefrikk oil field and well 34/10-32 in the Gullfaks Sør oil and gas field) and onshore (Fig. 12).

Since the amount of shear strain in the hanging walls to the main faults decreases with depth, the offset across the faults increases at deeper stratigraphic levels (see Fig. 7). In some cases, fault displacement at the top of the Brent Group may be only 10 m, whereas the displacement at the top of the Statfjord Formation may be as much as

Fig. 8. Stereonet plots of dip direction/dip from the different formations penetrated by well 34/10-8. Dip of bedding in the uppermost formations is to the west but decreases rapidly with depth. Within the Cook Formation, dip of bedding is to the east. This change in dip describes large-scale drag in a triangular zone on the hanging wall side to the main faults within the rotated fault blocks of the domino system. See Fig. 1 for location.

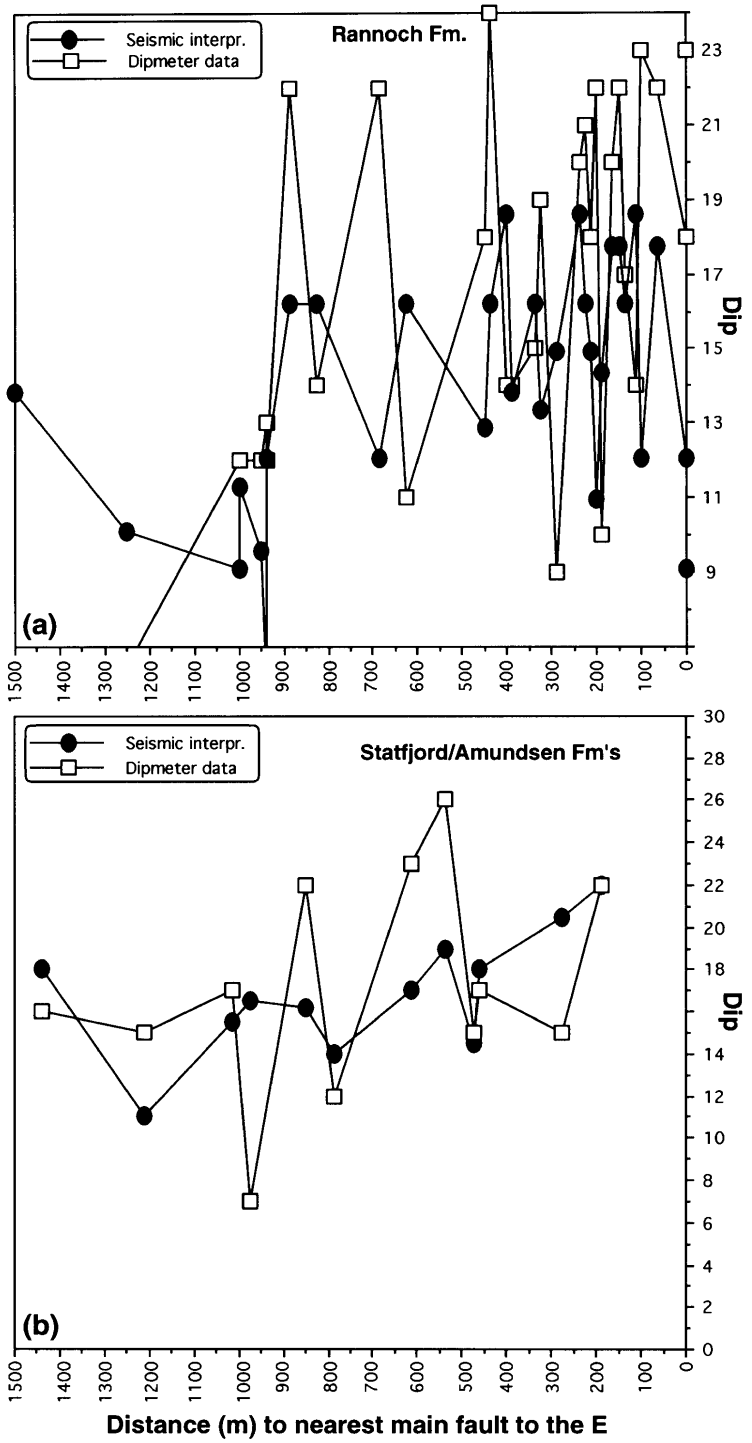

Fig. 10. Dip estimated from dipmeter data and from depth-converted seismic interpretation plotted against the distance to the nearest main fault to the east for the Rannoch Formation (a) and for the Statford/Amundsen Formation level (b) (domino area). Each data point represents a single well around which the dip is estimated from the seismic interpretation, and where the highest concentration of dip is estimated from dipmeter data. Both data sets show a clear decrease in dip to the west, consistent with the geometry shown in Fig. 1 (bottom), Fig. 3 and Fig. 7. A binomial test (with confidence interval of 95%) of the data indicates that dipmeter estimates are slightly higher than seismically determined dips in (a), while no systematic significant difference is detected for data shown in (b).

250 m. The reason that the deeper stratigraphic levels are less affected by large-scale drag is likely that these rocks were more consolidated at the time of deformation. In fact, since deformation of the Gullfaks area started immediately after deposition of the Brent Group, the sands of the Tarbert Formation were little or not con-

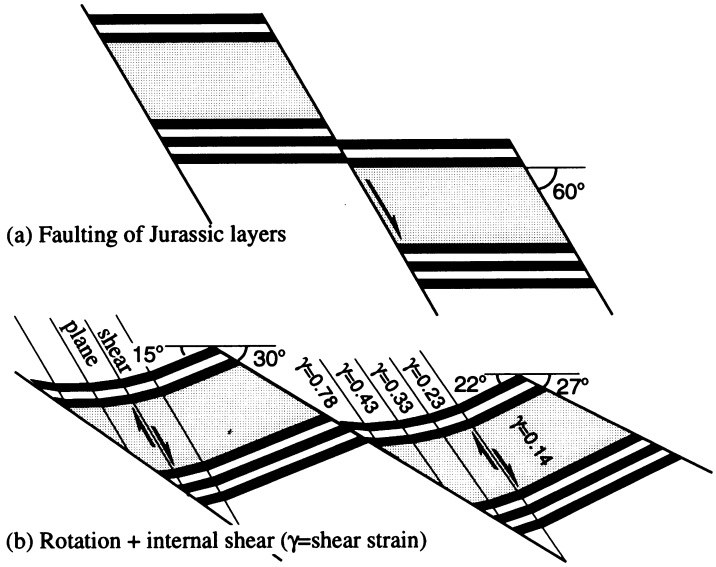

Fig. 11. The large-scale drag within the triangular zone may be easily explained by applying increasing shear strain towards the hanging wall side to the main fault. The shear angle is synthetic and somewhat steeper than the main fault. Thus, the amount of shear will decrease with depth as well as to the east.

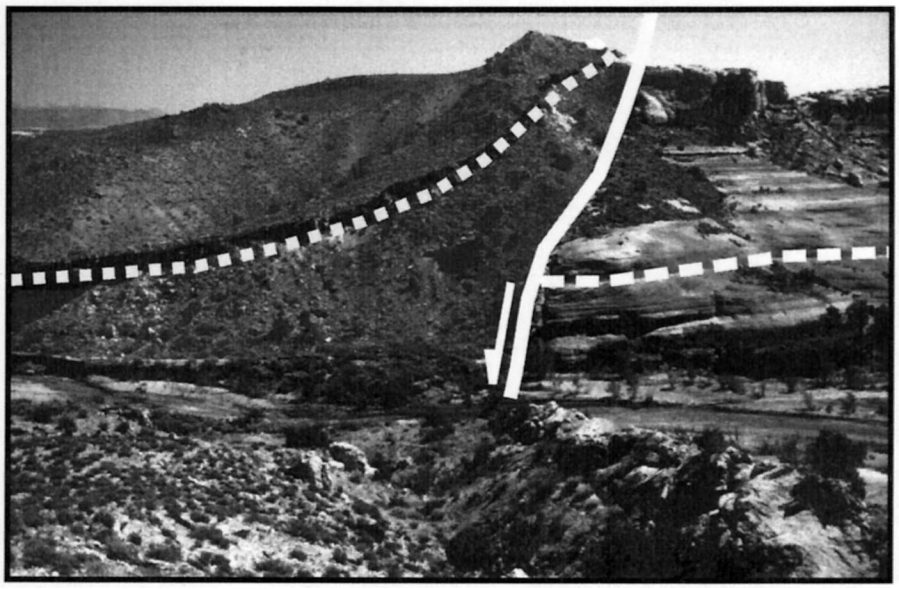

Fig. 12. Field example from the Bartlett fault near Moab, Utah. A large normal fault separates the massive Entrada sandstone (footwall) from interlayered sandstones and shales of the Cedar Mountain Formation (hanging wall). Strata in the hanging wall have developed a several hundred meter wide drag zone. The displacement along the fault is ca 300 m.

solidated at all and would therefore be less resistant against soft and ductile deformation

Wells located outside the triangular zone tend to show a downward increase in dip of bedding. Well 34/10-A-8 is located mainly in a footwall position to one of the main faults. The dip vs depth and dip direction vs depth plots (Fig. 13) show a change from shallow dip (ca 15°) to the southwest in the Tarbert Formation to steeper dip (ca 23°) to the west in the stratigraphically deeper Drake Formation. This small increase in dip with depth is thought to be related to differential compaction. After rotation of the layering within the domino fault blocks, the Jurassic and Triassic strata were overlain by several hundred meters of Cretaceous and Tertiary sediments. Loosely consolidated rocks of the Tarbert Formation was then more compacted and dips of layers thereby decreased more than those of the Statfjord Formation (Fossen and Hesthammer, 1998).

In some cases, the western boundary of the triangular zone is not defined by one of the main faults, but rather

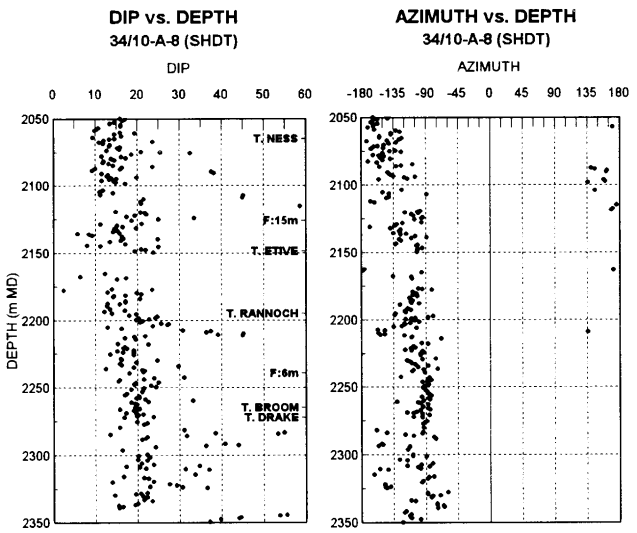

Fig. 13. The dip vs depth plot for well 34/10-A-8, which is located outside the triangular zone of large-scale drag, shows how amount of dip increases slightly with depth. See Fig. 1 for location.

by a minor fault (Fig. 14(b)) or simply by an abrupt change in dip (Fig. 14(a)), in which case the offset across the structure is entirely accommodated by continuous or ductile deformation. In these cases, the main fault is located farther to the west. The dip within several such 'high dip buffer zones' have been verified by dipmeter data (from wells 34/10-A-15, 34/10-A-25A, 34/10-A-27A, 34/10-B-8), showing that strata between the minor fault and the main fault to the west are not affected by large-scale drag, and are tilted in the direction of opening of the zone, typically to the north. Because strata are steep within the high dip buffer zone, the amount of shear strain is likely low (assuming that the rocks underwent a component of rigid fault block rotation so that a decrease in the dip of bedding represents an increase in shear strain; see Fossen and Hesthammer, 1998). This implies that the rocks on the hanging wall side of the main fault is no more deformed than the footwall at this stratigraphic level. Shear strain will however increase drastically across the minor fault or across the change in dip to the east. The 'high dip buffer zones' may possibly represent hard-linked relay-ramp structures (e.g. Trudgill and Cartwright, 1994).

5.2. *Faults*

Larger faults are usually identified both on seismic data and from stratigraphic well log correlation. From dipmeter data, the main faults within the domino system can usually be identified by the change in dip across the faults, as described above. The drastic change from shallow dips in the hanging wall to much steeper dips in the footwall is readily distinguished (Rønningsland, 1990). In areas where such a change in dip (triangular zone) does not exist, it is difficult to separate large-scale from minor faults based on dipmeter data alone.

Figure 15(a) shows dip vs depth and dip direction vs depth plots for well 34/10-C-6 which is located within the horst complex. Due to the high amount of scatter, it is hard to distinguish any break at 2820 mMD, which is the location of a fault with 82 m missing section. The cumulative dip plot (Fig. 15(b)), however, clearly shows a change in the gradient of the curve at about 2820 mMD. Above this depth, the curve has a relatively shallow gradient, suggesting a fairly rapid increase in the cumulative dip. Below the fault, the gradient is steeper, indicating shallower dip of bedding. This is consistent with observations from seismic data (Fig. 15(c)) where the hanging wall dips to the east, and the footwall is subhorizontal.

6. Small-scale structures

Dipmeter data are especially useful for identification of faults (Werner et al., 1987; Koepsell et al., 1989a; 1989b; Devilliers and Werner, 1990; Zhang, 1993), particularly those below seismic resolution, since it is commonly difficult to obtain information of the fault's geometry by other means (Adams et al., 1992). In the Gullfaks Field, faults are commonly associated with a gradual or abrupt change in amount of dip and/or dip direction of bedding. If no such changes exist, it is normally not possible to detect faults from dipmeter data alone. Similarly, dipmeter data alone can not separate between a fault and an unconformity in those cases where abrupt changes occur. The cumulative dip and dip direction plots (Fig. 15(b); Hurley, 1994) are especially suitable for recognising faults where dip of strata changes abruptly across the fault plane, whereas the statistical curvature analysis technique (Bengtson, 1981; see also Kaya and Norman, 1993) provides the best mean for recognising and describing drag features. Stereonet plots are generally not suitable for fault detection, since they do not yield information on changes in dip and azimuth with depth.

Figure 16 shows an example of local drag (affecting some tens of meters on each side of the fault plane) related to a fault with 9 m missing section within the Amundsen Formation in well 34/10-C-3. Whereas well log correlation has placed the fault at 2721 mMD, dipmeter data suggest that the zone of highest shear strain is located at 2713 mMD. It is thus likely that the location of the fault is slightly misplaced by stratigraphic well log correlation. The interval affected by drag in this case covers an area of approximately 100 m and is not easily observed on seismic data. Analyses of dip *direction* of drag-folded bedding give an indication of the fault orientation (the bedding within the drag zone is usually rotated towards parallelism with the fault). Since there is no apparent change in dip direction of the bedding in Fig. 16, it is

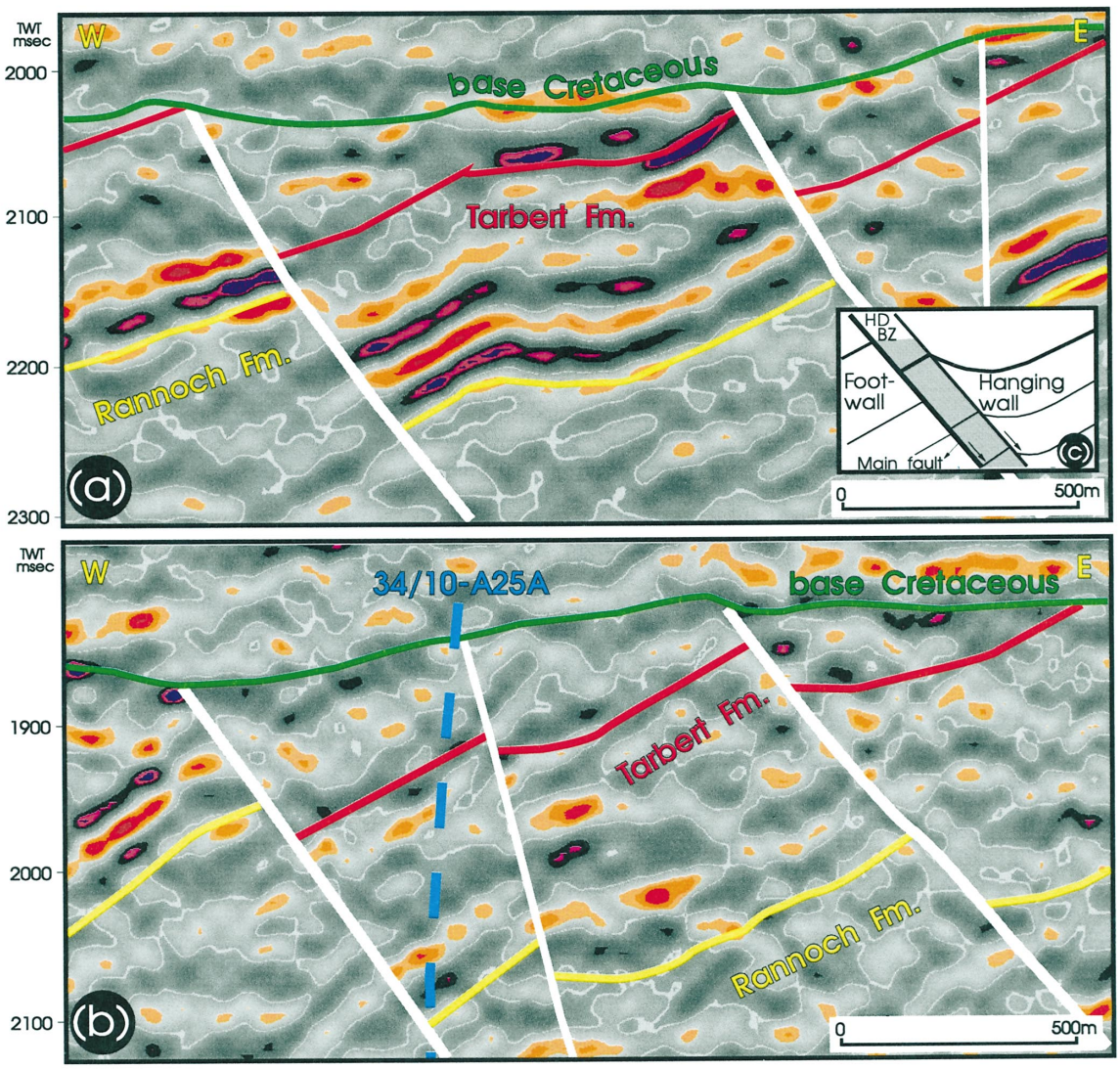

Fig. 14. Several places within the domino system, the large-scale drag terminates against a minor fault rather than against the main fault which is located farther to the west. Between the minor fault and the main fault is a zone of high dip, termed the 'high dip buffer zone'. Figures (a) and (b) show two seismic sections through two such zones. (c) Schematic illustration of the high dip buffer zone.

likely that the fault dips to the west. The amount of dip increases to 40° or more at the location of the fault. This increase in dip towards the location of the fault is termed 'steepening drag' (Bengtson, 1981), and occur when both bedding and the fault dip in the same direction. Since bedding is bent towards parallelism with the fault plane, this gives a minimum estimate of the amount of dip of the fault plane. It is thus possible to achieve an understanding of the geometry of bedding around a fault as well as the orientation of the fault plane itself.

It is important to try to quantify the effect of drag as it may affect the prediction of stratigraphic juxtaposition and fault-sealing potential. A geological profile through well 34/10-C-3 was constructed based on the dipmeter information from the well (Fig. 17). Dip isogons are drawn parallel to the fault, and the orientation of the fault is estimated from the dip and azimuth vs depth plots. Although the missing section is only 9 m, the result shows that the total offset of layering outside the area affected by drag is more than 100 m. The example clearly illustrates the importance of such geometries.

A similar example is seen in well 34/10-A-5H (Fig. 18). A fault with 17 m missing section has been identified from well log correlation. The area affected by drag covers an interval of approximately 50 m along the wellbore hole. Strata above the fault dip shallowly to the west. At approximately 1930 mMD, the apparent dip decreases to zero before it increases again, this time to the east. Below 1955 mMD, the trend becomes a mirror image of that above. This pattern of flattening drag (Bengtson, 1981)

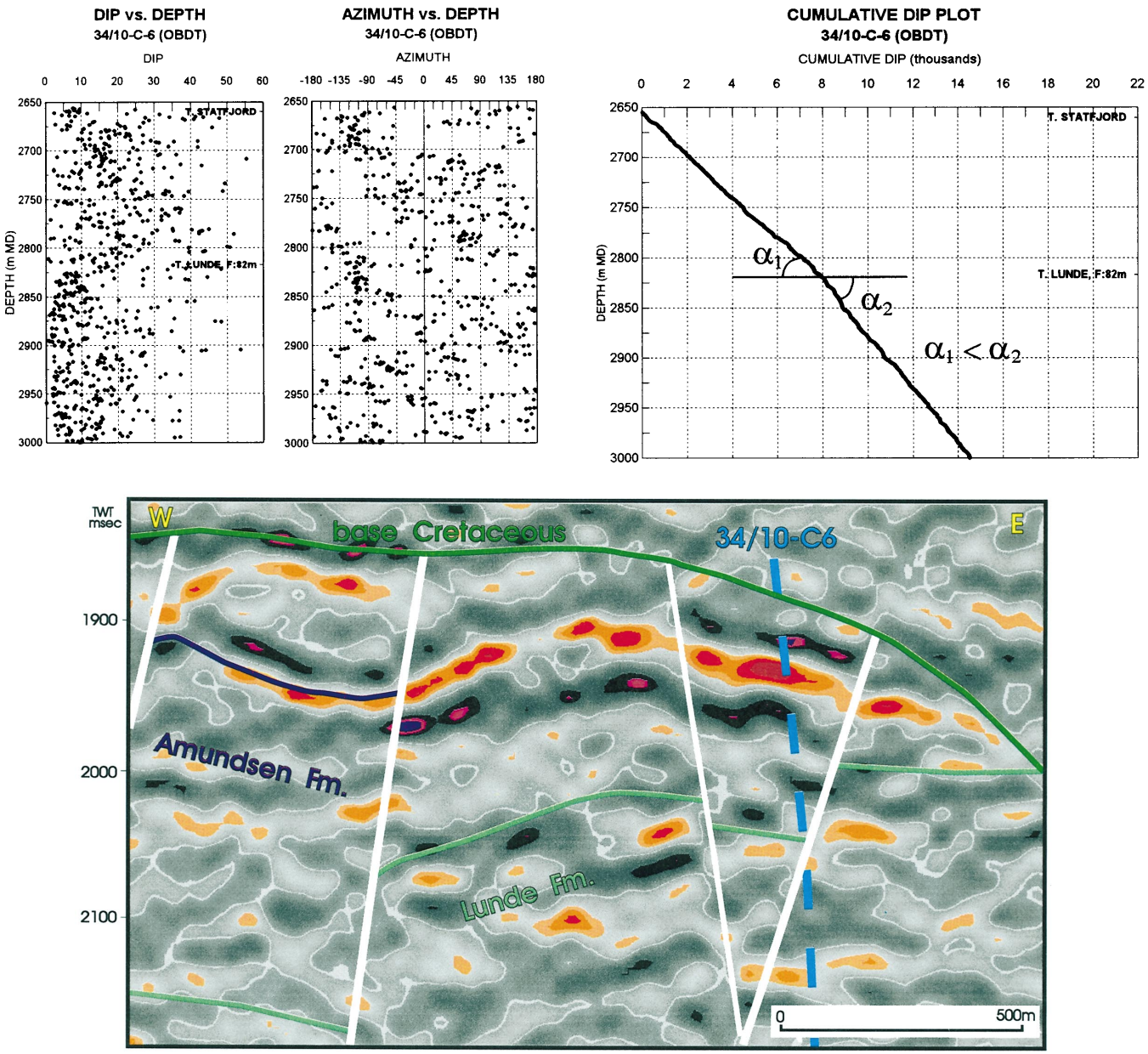

Fig. 15. (a) The dip vs depth and azimuth vs depth plots for well 34/10-C-6 show much scatter. It is difficult from these data to observe the fault with 82 m missing section identified from well log correlation. (b) The cumulative dip plot (Hurley, 1994) shows a clear change in gradient at the location of the fault. This type of plot can thus help in the identification of faults where data quality is poor. (c) A seismic profile through well 34/10-C-6. The observations from dipmeter data (a-b) are consistent with observations from seismic data. See Fig. 1 for location.

is caused by dragging of west-dipping strata towards parallelism with an east-dipping fault. Before strata can dip to the east, it must first be subhorizontal.

A second fault with 31 m missing section has been identified in well 34/10-A-5H at 1979 mMD. This fault has no related drag structures, and can only be identified from dipmeter data by a drastic change in amount of dip (especially apparent on the longitudinal dip component plot; Fig. 18). Without the help of well log correlation and detailed knowledge of the sedimentology in the reservoir, such a break in amount of dip could be mistaken for an unconformity or a sequence boundary.

When the location of a minor fault is known, stereonet plots can be made for the interval above and below the fault. In an example from well 34/10-A-11 (Fig. 19), dip of strata above a fault (hanging wall) with 10 m missing section is somewhat steeper than dip of bedding below the fault (footwall). This difference is related to drag in the hanging wall, whereas the footwall is hardly affected by drag. The dip of strata in the footwall is therefore

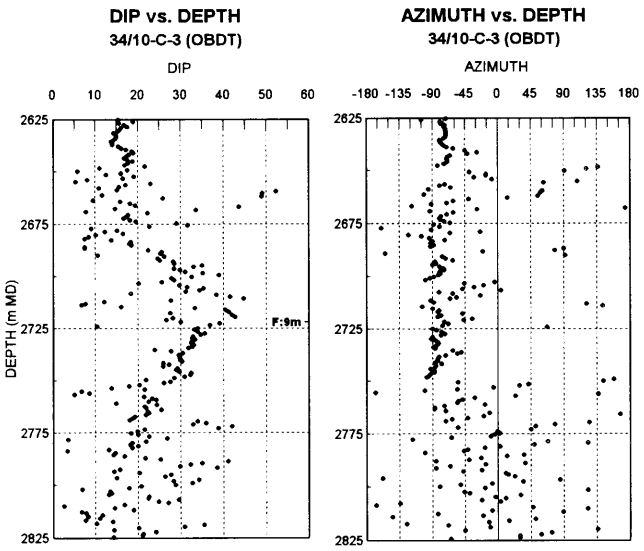

Fig. 16. The dip vs depth and dip direction vs depth plots for well 34/10-C-3 clearly identify an area of steepening drag (Bengtson, 1981) related to a fault with 9 m missing section. The dip direction is to the west at all depths. See Fig. 1 for location.

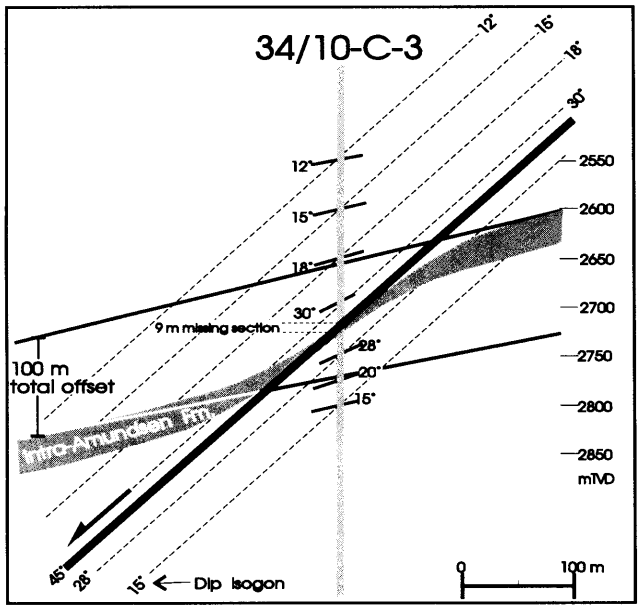

Fig. 17. An exercise was carried out on dipmeter data from well 34/10-C-3 in order to quantify the amount of missing section relative to total offset. The results show that, where drag is present, the total offset may be more than one order of magnitude larger (100 m) than the missing section recorded by well log correlation (9 m).

more consistent with the general dip of bedding in the area.

In order to check for more systematic differences in deformation between the hanging wall and footwall of minor faults, the average intervals affected by local drag on both sides of 46 faults where examined. The result (Fig. 20) shows that the interval affected by drag is more

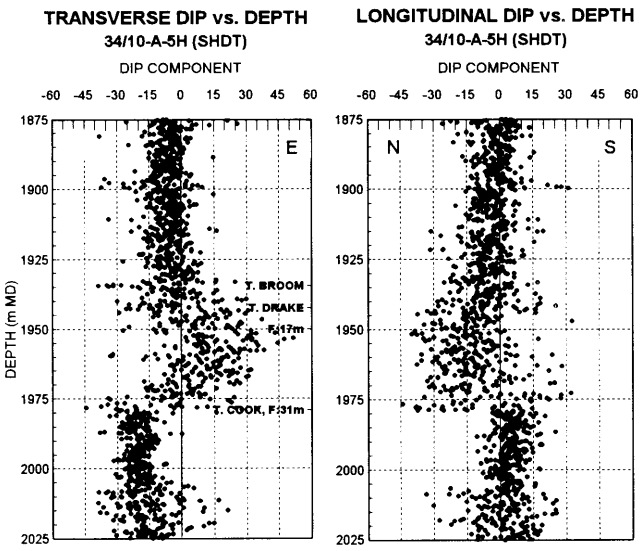

Fig. 18. Transverse and longitudinal dip component plots for parts of well 34/10-A-5H. The plots show apparent dip of the formation for a chosen profile direction (105° for the transverse dip component plot and 015° for the longitudinal dip component plot). This display method was first documented by Bengtson (1981) and allows for analyses of the curvature of structures such as folds and faults. A fault with 17 m missing section, located at 1955 mMD, is associated with a zone of flattening drag which is easily identified on the transverse dip component plot. The fault located at 1979 mMD is clearly not associated with such a zone of drag. Instead, the fault is identified from dipmeter data by a change in amount of dip. This is seen best on the longitudinal dip component plot where the bedding above the fault dips in a northerly direction whereas bedding below the fault dips in a southerly direction. See Fig. 1 for location.

than twice as wide in the hanging wall (average of 60 m along the wellbore) than in the footwall (average of 29 m) for all formations.

Figure 20 does not indicate any significant differences in the interval affected by drag between the different formations. These formations range from thick sandstone units (Tarbert, Etive, Rannoch, Cook and Statfjord Formations), via interlayered sandstones and shales (Ness Formation), to thick shale units (Drake and Amundsen Formations). There is thus no clear correlation between lithology and width of the drag zone. This is likely due to the fact that the sandstones were poorly consolidated at the time of deformation, and therefore had shear strengths close to that of shale.

When deformation started, the bedding was more or less horizontal. The vertical axis in Fig. 20 therefore also reflects increasing depth at the onset of deformation (the Statfjord Formation was located deeper than the Brent Group prior to the deformation). With the possible exception of the Statfjord Formation (where only three faults with associated drag were identified), there is no significant correlation between the average interval affected by drag and the depth at the time of deformation.

A comparison of formation vs the normalised number of faults with related drag is shown in Fig. 21(a). From

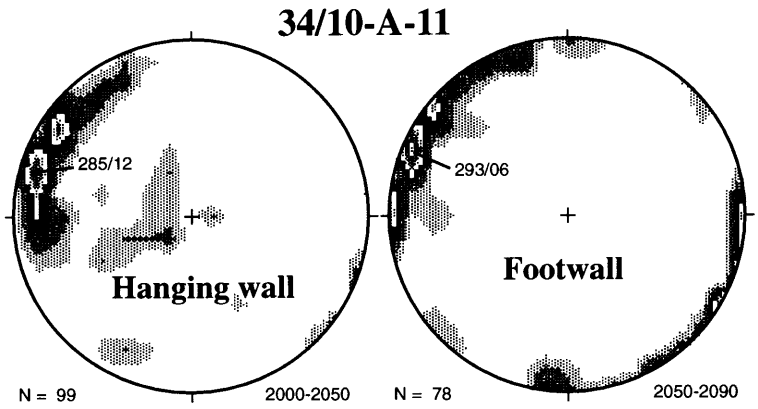

Fig. 19. Stereonet plots of dip direction/dip of bedding from the hanging wall and footwall of a minor west-dipping fault penetrated by well 34/10-A-11. Dip of bedding in the hanging wall is clearly steeper than dip of bedding in the footwall. This is consistent with steepening drag related to a west-dipping fault. See Fig. 1 for location.

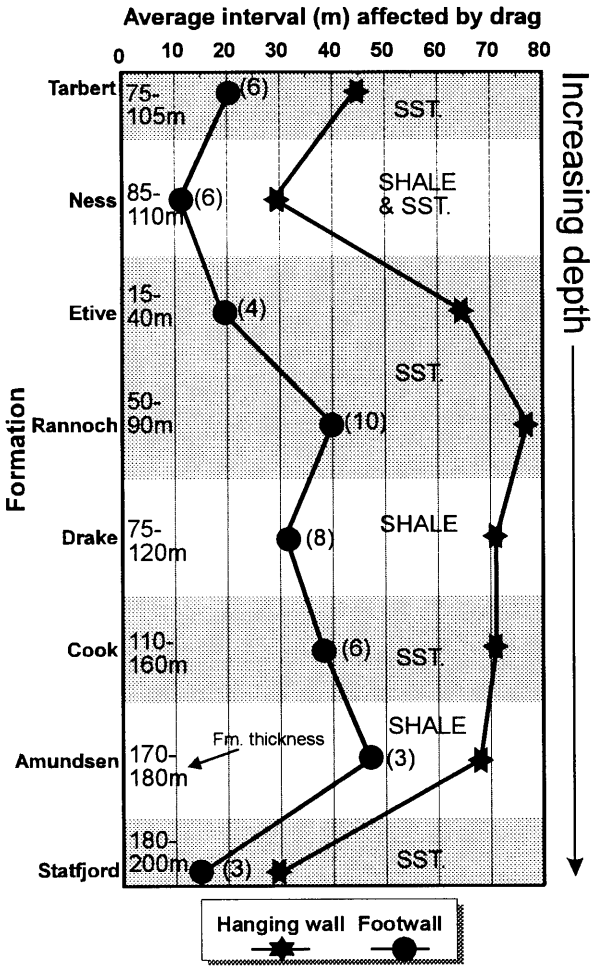

Fig. 20. Average interval (measured along the wellbore hole) affected by drag for various formations clearly demonstrates that the deformation in the hanging walls to the faults affects a much wider interval than in the footwalls. No clear relationship is seen between lithology and width of the drag zone. Since the width of the drag zone is measured along the trace of the wells, which is not necessarily perpendicular to the fault, the intervals represent maximum estimates.

this plot, it appears to be fewer faults at deeper stratigraphic levels that have developed associated drag. This finding suggests that the lithologies at deeper stratigraphic levels were somewhat more consolidated than shallower strata at the time of deformation, and is consistent with the observation that large-scale drag (triangular zone) is more widespread in the upper parts of the reservoir. The ratio between faults with identified drag from dipmeter data and faults without drag (identified by other means) is plotted in Fig. 21(b). The figure indicates that faults within the shales of the Drake and Amundsen Formations are less likely to exhibit drag. Drag folding associated with faulting is most commonly observed within the Ness, Rannoch and Statfjord Formations. A total of 52 faults with related drag were identified from dipmeter data. In comparison, 83 faults have been identified from other well log correlations within the same intervals. This gives a weighted ratio of 0.63, and suggests that drag is associated with more than half of all faults in the Gullfaks Field.

In most cases where the faults are associated with drag folding, it is possible from dipmeter data to indicate the dip direction of the faults. The results from analyses of 39 faults on the Gullfaks Field is illustrated in Fig. 22(b). Almost the entire population (32) of faults with associated drag dips either in an easterly (most common) or westerly direction. Very few north- or south-dipping faults exhibit drag zones. This is partly due to the general strike of bedding which is also to the north (it is easier to change only the amount of dip rather than both dip and azimuth). Also, easterly trending faults commonly show a strike-slip component (Rouby et al., 1996), which will prevent the development of drag folds. Although drag folds with north-trending fold axes are most common, dipmeter data are capable of recording drag features which involves changes in both dip and azimuth (Fig. 23).

The average E–W density for ca N–S trending faults with related drag is 4.6 per km (32 faults within 6.9 km

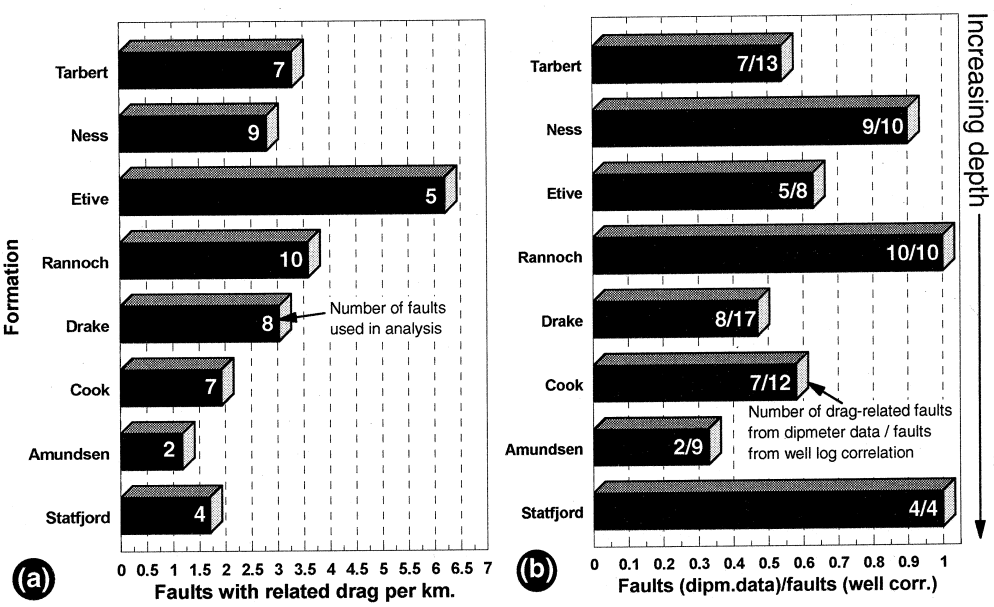

Fig. 21. (a) Plot of faults with related drag per kilometre with respect to lithology. Fewer faults appear to have developed associated drag at deeper stratigraphic levels. (b) A plot of the relationship between drag-related faults identified from dipmeter data and faults identified from well log correlation (same interval) with respect to the different formations does not support the common assumption that drag is more common in shales than in sandstones. Instead, drag is less commonly observed in the shaly Drake and Amundsen Formations.

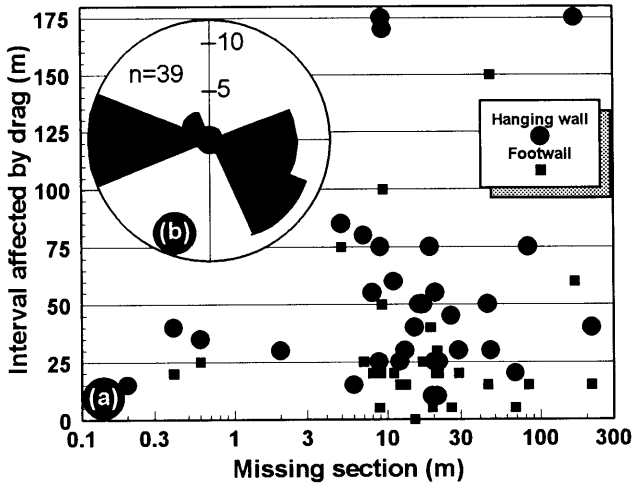

Fig. 22. (a) X–Y scatter plot showing interval of strata affected by drag near faults vs missing section. There is no clear relationship between interval affected by drag and the size of the fault as identified from missing section. (b) A plot of the dip direction of faults as identified from dipmeter data (based on associated drag of bedding) shows that most faults that developed associated drag dip to the east (most common) or the west.

of analysed dipmeter data in E–W direction). The density of *all* faults in E–W direction as identified from well log correlation is 4.4 per km (237 faults within 53.8 km of drilled reservoir in E–W direction). It is thus likely that, due to the effect of drag and little missing section, not all faults are identified from routine well log correlation.

A plot of missing section vs interval affected by drag (Fig. 22(a)) reveals no significant correlation. From this plot, it is clear that large-scale faults do not necessarily develop wider local drag zones than minor faults. In fact, with the exception of the domino system where the main faults are associated with a triangular zone of large-scale drag, there are surprisingly few differences between large-scale and small-scale faults in terms of change in dip and azimuth of bedding and width of the local drag zone. This important observation suggests that local drag started to develop prior to the initiation of the fault plane, or as a process zone ahead of the growing fault surface (Hobbs et al., 1976; Scholz et al., 1993). In this model (Fig. 24), a fault plane develops when the amount of shear strain (related to displacement across the drag zone and its width) exceeds a critical value. This is so because ductile deformation (at some scale) is only feasible until the critical strength of the rock is exceeded and a fracture forms. After this point, deformation is more easily accommodated by slip along the fracture (brittle faulting) than by ductile deformation in the vicinity of the fracture. Deviations from this idealised model may be explained by changes in the geometry and kinematics of the fault zone during the slip history.

7. Integrated use of well data and seismic attribute maps

Recognition of faults and related structures at the limit of, or below seismic resolution, is perhaps the largest challenge for structural geologists involved in oil fields under production. Down-scaling of assumed self-similar fault attributes have been applied in some cases (e.g.

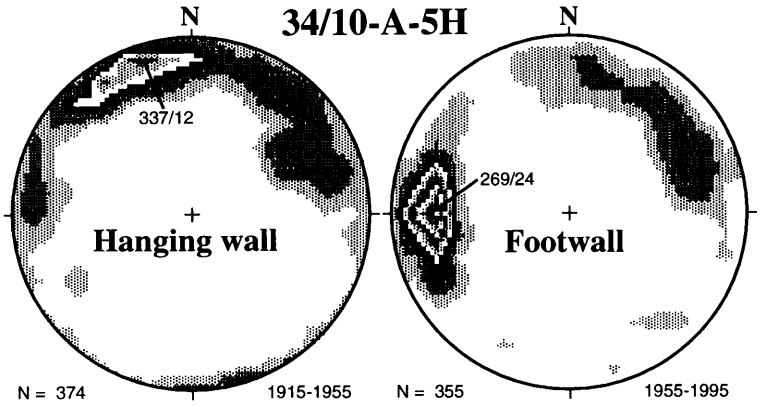

Fig. 23. Stereonet plots of bedding orientation (dip direction/dip) for the hanging wall and footwall of a minor fault penetrated by well 34/10-A-5H (see Fig. 1 for location). The figure shows clear differences in dip of strata in the hanging wall (shallow dips to the northwest) and footwall (steeper dips to the west). In addition, there are clear evidence of drag in a northerly direction. Drag is to the northeast, suggesting a northeast-dipping fault.

Gauthier and Lake, 1993). A statistical study of fault populations in the Gullfaks Field (Fossen and Rørnes, 1996) indicates that this approach would not be appropriate in the Gullfaks area. However, integrated use of the large number of dipmeter data, other well data and seismic data enables us to approach this problem without the use of statistical fault scaling models (Hesthammer, 1998a; 1998b).

Seismic attribute analyses have helped to detect faults with displacements, in some cases, down to 5 m, although conventional 3D seismic interpretation typically allows only identification of faults with displacements more than 15–25 m. Seismic timedip maps of the strong intra-Ness Formation reflection show abundant (curvi-)linear features (Fig. 25). These approximately N–S trending features are especially numerous in the eastern (footwall) parts of the domino fault blocks, and relief maps indicate that most (ca 85%) are directly associated with down-to-the-west offsets of seismic reflections (Hesthammer and Fossen, 1997a). If the linear features represent minor faults, it would indicate that the footwalls of the rotated domino fault blocks are more deformed than the hanging walls and that the deformation occurred along discrete west-dipping faults and associated fault block rotation. However, there are several reasons why such an interpretation may not be valid. For example, structural modelling for the Gullfaks domino system (Fig. 11) suggests that most deformation is located in the hanging wall part of the domino fault blocks. In addition, the average density in E–W direction of the west-dipping seismic features is approximately 9 per km (estimated from timedip maps of the intra-Ness and top Statfjord Formations; Hesthammer and Fossen, 1997b). Most of the (curvi-)linear features are related to apparent offset of reflections in the range of 10–30 m. Generally, all faults with offsets in this range can be identified by well log correlation (Fossen and Rørnes, 1996). The significantly lower fault density calculated from well log data, 2.1 or 4.4 per km if the number of faults is divided by the amount of drilled reservoir projected into an E–W direction, indicates that many do not represent faults (note that the method of dividing the total number of faults identified from well log correlation by an amount of well data projected into any direction will result in a too high number of faults per km). In addition, recent studies of 152 faults with displacement less than 30 m that have been penetrated by wells on the Gullfaks Field demonstrate that less than 25% of these faults can be observed in the seismic data. Structural analyses of 6 km of core data (work in progress) are consistent with the above observations and suggest that 'ductile' and widely distributed grain reorganisation rather than discrete micro-faulting is responsible for most of the deformation within the domino system on the Gullfaks Field.

Detailed analyses of dipmeter data give further support to this conclusion. Analyses show that approximately 60% of all faults detected by stratigraphic well log correlation have developed local drag, and that drag is preferentially related to N–S trending faults (i.e. considerably more than 60% of N–S trending faults have developed local drag). Most of the N–S trending faults are therefore detectable from dipmeter data. Twelve west-dipping (dip direction is $270+/-22.5^{\circ}$) faults have been identified from dipmeter data on the basis of drag, i.e. an average density per km of 0.5, or 1.8 if projected onto an E–W section (a total of 6.9 km of analysed dipmeter data exists in an E–W direction; see Table 1 for detailed explanation). Assuming that 80% of the N–S trending faults developed drag, about 50 faults should have been identified from dipmeter data if all the (curvi-)linear features with associated down-to-the-west offset (density = 9 per km) observed on the timedip maps were faults.

Another approach is to compare apparent dip at the seismic and sub-seismic scales. If subseismic faults exist, the dipping layer (reflection) will be imaged with an averaged dip on a seismic section, while the true dip of bed-

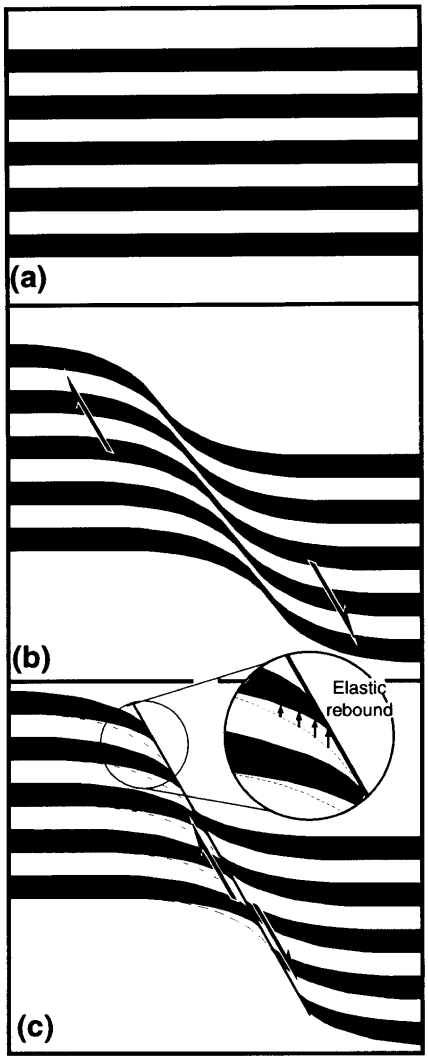

Fig. 24. Schematic illustration of how a layered sequence (a) may be deformed by localised shearing (b) to form a zone of drag. Eventually the deformation results in discrete slip (a fault) along the line of maximum shear deformation (c). Given that tensional stresses give rise to horizontal extension across the zone, the drag is expected to decrease after the establishment of the fault due to rebound of the elastic component of strain associated with the drag structure.

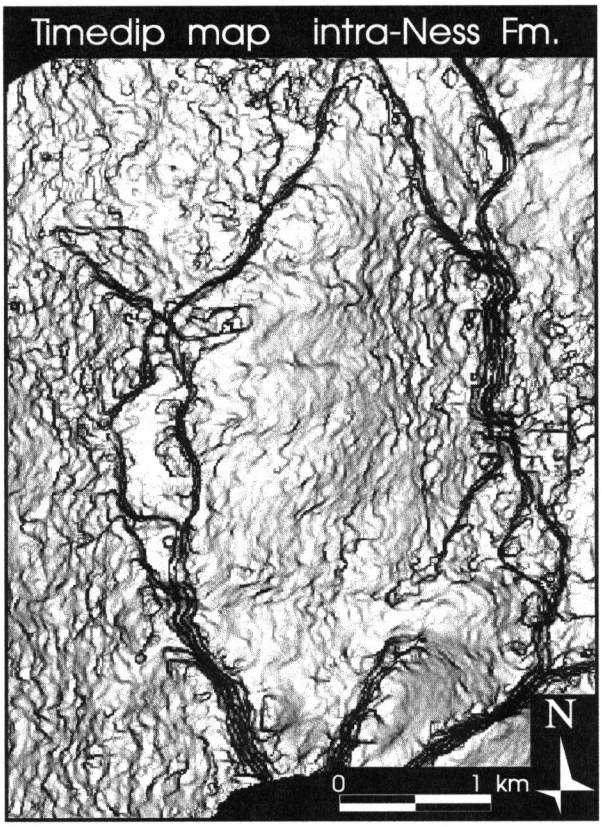

Fig. 25. Timedip map of an intra-Ness Formation reflection. Most of the N-S trending (curvi-)linear features observed on the dip map result from interference of dipping coherent noise with the intra-Ness Formation reflection. See text for discussion.

ding may be lower or larger, depending on the geometry of the sub-seismic faults (Fig. 26). This prediction can be demonstrated by comparing dip from dipmeter data and seismic interpretation. If the true dip is detectable from dipmeter data, then this dip must generally be different from that detected from seismic interpretation. Furthermore, if the (curvi-)linear features reflect sub-seismic faulting, the amount of dip from dipmeter data should be lower than the seismically interpreted dip (Fig. 26). Figure 10 showed a comparison of dip from dipmeter data and seismic dip for the Rannoch and Statfjord Formations. Statistical analysis shows that dip from dipmeter data is slightly *higher* than seismic dip for the Rannoch Formation (Fig. 10(a)), whereas no significant difference exists for the Amundsen and Statfjord Formations (Fig. 10(b)). This finding indicates that, while there may be some support for minor east-dipping faults, minor west-dipping faults are relatively uncommon, and not comparable to the high distribution of (curvi-)linear features on the attribute maps. Hence, we conclude that much of the intra-block deformation is not reflected by dipmeter data, and thus occurs on a very small scale. Complementary core analysis indicates that much deformation is by 'ductile' grain-reorganisation processes, particularly in the Brent Group which was very poorly consolidated during deformation.

We suggest that the (curvi-)linear features observed on the seismic timedip maps are related to the interference of dipping coherent noise with real reflections (Hesthammer and Fossen, 1997a; 1997b; Hesthammer and Løkkebø, 1997; Hesthammer, 1998b). The effect of this interference is clearly demonstrated in Fig. 27, which shows a seismic profile through exploration well 34/10-5. Until recently, the 34/10-5 area was believed to be affected by footwall collapse with the presence of two east-dipping minor faults (Fig. 27(a)). Bedding within these two collapsed fault blocks was, based entirely on seismic data, interpreted to be to the west. However, dipmeter data clearly

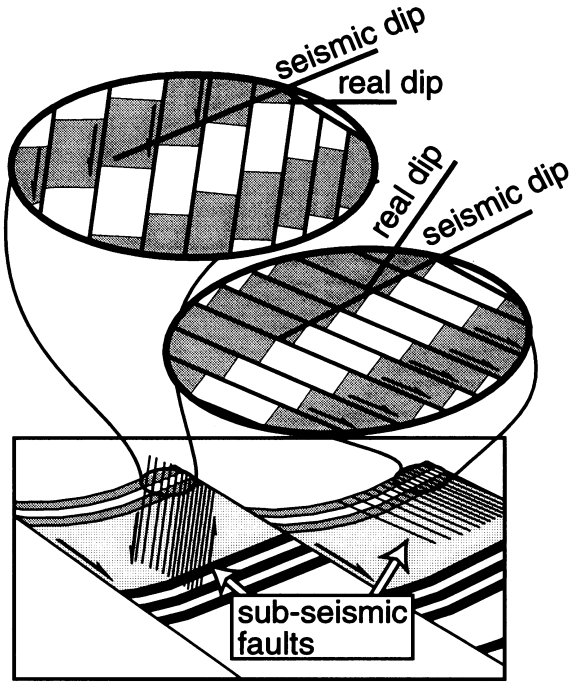

Fig. 26. Cartoon showing that if the features observed on a seismic timedip map in the footwalls to some of the rotated fault blocks in the domino system represented faults, dip from dipmeter data should be different from seismic dip. Thus, by comparing dip from dipmeter data with seismic dip, it is possible to obtain information on shear angle within the fault blocks provided that the strain was accommodated by discrete faulting rather than by a more widely distributed homogeneous grain reorganisation.

show that bedding within the two fault blocks is subhorizontal (Fig. 27(b)). The area was thus reinterpreted based on the dipmeter data. In the section above the base Cretaceous unconformity where layers are known to be subhorizontal (Fig. 27(c)), it is clear that the interference of west-dipping coherent noise (the seismic data set contains abundant west- and east-dipping coherent noise) with a subhorizontal reflection causes apparent rotation of the reflection, and the appearance of west-dipping strata. This example demonstrates how important it is to use all available data to distinguish between real seismic reflections and seismic noise, and how dipmeter data combined with seismic data can be used to approach this common type of problem in reservoir characterisation.

8. Implications for oil production

The observation that the hanging wall is generally more deformed than the footwall has implications for well planning in the Gullfaks Field and in structures that evolved under similar circumstances. While oil producers may be placed very close to the main faults in a footwall position, the wider zone of shear deformation in the hanging wall may make it necessary to place injectors farther away from the main fault. This is particularly important where fluid flow might be restricted by deformation structures (faults with several meters displacement and associated deformation bands) in an E–W direction, e.g. where minor faults within the triangular zone are parallel to the east-dipping shear planes. Pressure and production data indicate that this may be the case in the Gullfaks Field. In addition, collapsed pore space in the large-scale drag zone may reduce permeability in the hanging wall. The onshore analogue example from Utah (Fig. 12) shows a 300–400 m wide drag zone in the hanging wall to a normal fault with 300 m displacement. Silica-rich fluids have cemented the rocks in the drag zone, while the almost undeformed sandstones in the footwall have retained their original porosity a few meters away from the fault. A similar situation may exist in the hanging walls to two main faults on the Gullfaks Field, where wells 34/10-C-31 and 34/10-B-36 have shown highly calcite-cemented reservoir rocks.

We have described a downward decrease in the amount of large-scale drag in the hanging walls to the main faults in the Gullfaks Field, resulting in increasing throw with depth. For example, for a fault with only a few meters missing section at the upper Brent Group level, the throw at the Statfjord Formation level may be as much as 250 m. This will affect communication across the fault and must be considered when planning additional wells in deeper strata.

Figure 14 demonstrated the presence of a zone of high dip possibly related to a relay structure. The amount of shear strain within this zone is likely much lower than in the low-dip zone immediately to the east. When placing an injector within the 'high dip buffer zone', fluid flow may be preferentially in the opening direction of the zone (generally to the north), limited by the highly sheared zone and/or minor fault to the east, and the main fault to the west.

The presence of local drag, which should not be confused with large-scale drag observed within the triangular zone (Fig. 7), is also of importance in oil production. Missing section estimated from standard well log correlation methods does not account for the effect of drag. Also, local drag is usually not identified from seismic data due to resolution limitations. Consequently, seismic interpretation of faults intersected by wells will commonly be based on amount of missing section reported by the sedimentologists. The result may be that the measured missing section may be much less than the total offset measured outside the zone affected by drag (Fig. 17). Due to the effect of drag, a well located in the hanging wall may intersect the interpreted horizon significantly deeper than planned. Similarly, a well located in the footwall may penetrate the strata at shallower levels than expected. In the example from well 34/10-C-3 (Fig. 17), the missing section was estimated to only 9 m, whereas the total offset of layering outside the area affected by drag is more than 100 m. When more than half of all

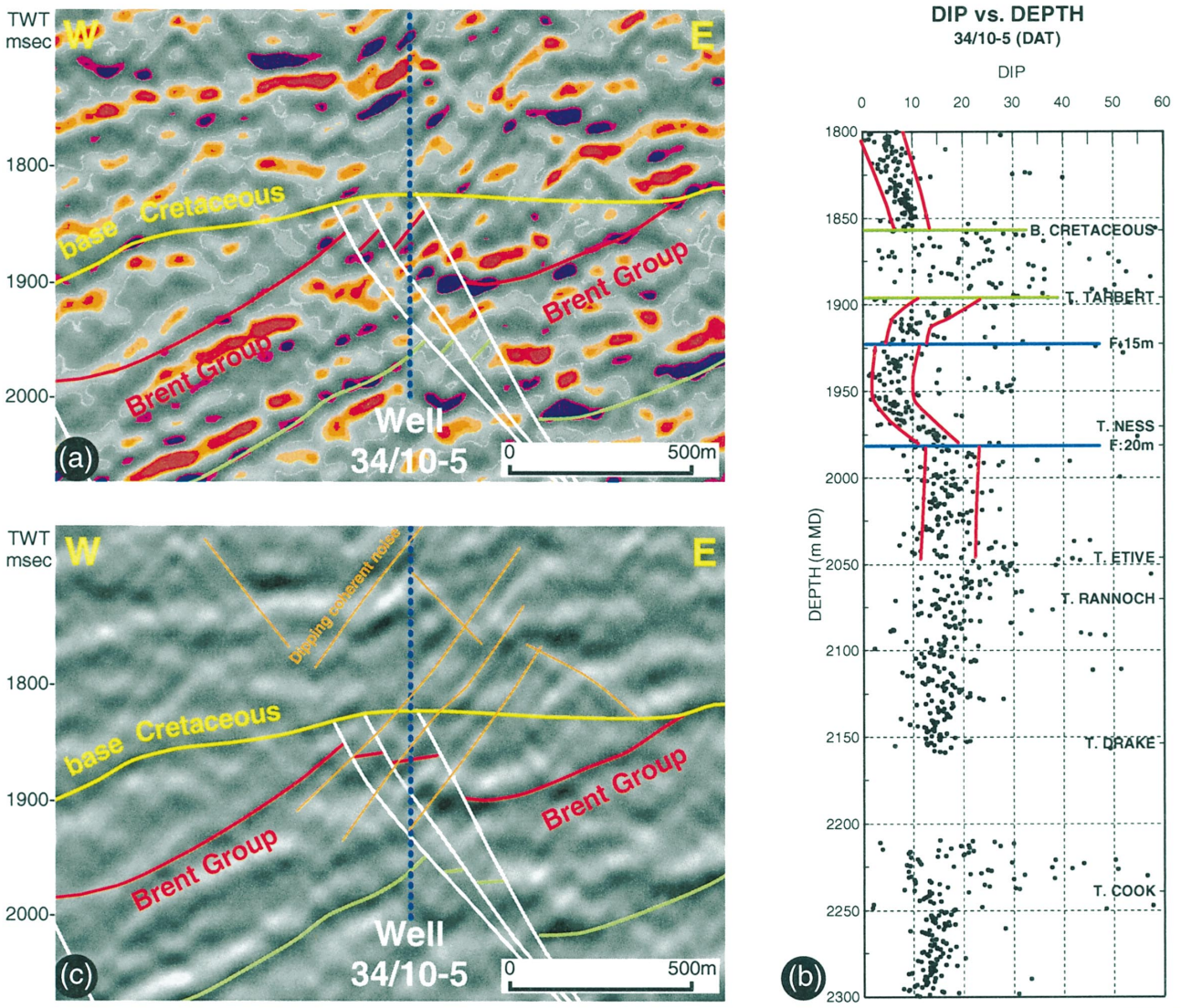

Fig. 27. (a) Seismic interpretation of footwall collapse around well 34/10-5 before the incorporation of available dipmeter data. (b) Dipmeter data show that dip of bedding within the two fault blocks is subhorizontal, and not west-dipping as indicated on seismic data. (c) Seismic data show the presence of dipping coherent noise above the reservoir. Within the reservoir, this noise interferes with subhorizontal reflections and causes the appearance of west-dipping strata. See Fig. 1 for location.

faults the Gullfaks Field have associated drag, this effect must obviously be considered during well planning and interpretation of seismic data.

Drag is also important when calculating sealing capacities of faults. Estimating sealing potential involves the use of structure maps from seismic interpretation and construction of fault juxtaposition diagrams (e.g. Knipe, 1997; Needham et al., 1996). Such estimates will generally not take into consideration the effect of local drag, since this is not observed in the seismic data. Whereas the total offset across a fault structure may predict a sealing sand-to-shale contact, the presence of drag may provide a communication path for the fluids (Fig. 28). Alternatively, where a sand–sand contact is expected, drag of a shale layer between the two sandstone units may destroy communication between these two units. Calculations of a faults sealing potential ideally should therefore not be based purely on seismic interpretation, where the effect of local drag is not easily observed. Drag also represents a potential source of error in statistical analysis of fault populations (e.g. Walsh and Watterson, 1987) which may be used in reservoir models. Detailed analysis of dipmeter data may offer a means of compensating for such possible errors.

9. Conclusions

Integrated use of dipmeter data helps to constrain the structural interpretation, particularly where the seismic

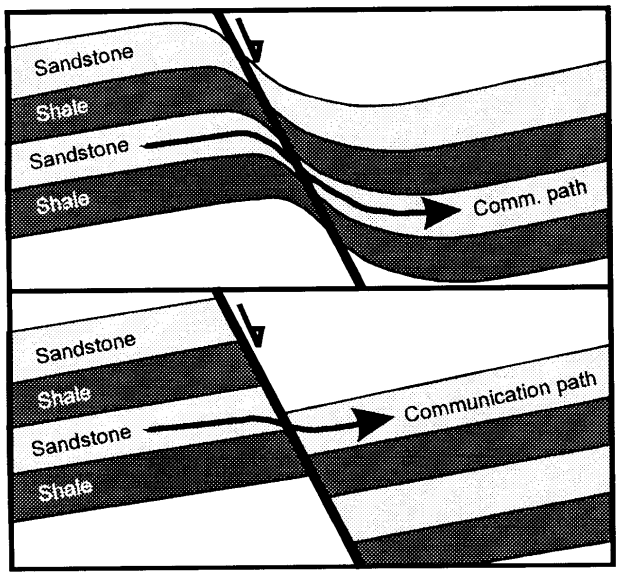

Fig. 28. The presence of local drag may give rise to communication across a fault which from seismic interpretation appears to be sealing. Also, drag of a shale layer may in some cases restrict communication between two sand units. The lower figure shows the results if no drag is associated with the fault.

data quality is poor and generally where smaller structures cannot be resolved seismically. The analyses of 23 km of dipmeter data from 48 wells on the Gullfaks Field, northern North Sea, have proven invaluable for a thorough understanding of the structural complexity and evolution of the field. Even where dipmeter data show much scatter, statistical analyses may give important information on variations in bed geometry. In the Gullfaks example, the general structure as interpreted from 3D seismic data is confirmed. However, dipmeter data have resulted in local reinterpretations and helped describe bedding and fault geometries in more detail. In particular, subseismic geometries are revealed and/or understood by the integrated use of dipmeter data, well log correlation data, core data, and seismic data. The following main points are emphasised:

(1) Dipmeter analyses from the Gullfaks Field verify the existence of three structural domains; the domino system, the horst complex and the accommodation zone.
(2) Dip of bedding within the rotated fault blocks of the domino system decreases towards the main faults to the west as a result of large-scale drag. The drag is caused mainly by some mechanism other than brittle faulting, probably by a widely distributed (ductile) flow at the grain scale. The effect of large-scale drag decreases with depth, due probably to a downward increase in the degree of consolidation at the time of deformation. In some areas of the Gullfaks Field, a 'high dip buffer zone' of low internal shear strain separates the triangular large-scale drag zone and the main fault to the west.
(3) Dipmeter data help the interpretation of seismic attribute maps, and indicate that most curvilinear features on timedip maps from the Gullfaks Field represent seismic noise rather than small faults. This conclusion is consistent with independent field data, and is consistent with the conclusion that much of the deformation was by grain reorganisation rather than discrete faulting. North-trending minor (and major) faults are most common and will restrict fluid flow in an E–W direction.
(4) Dipmeter data show that more than 60% of all faults on the Gullfaks Field are associated with local drag. Drag is not common for minor E–W trending faults, probably because they are internal accommodation structures influenced by lateral slip.
(5) The total offset across the complete fault/drag zone may be as much as one order of magnitude larger than missing section identified by well log correlation. The interval affected by drag is wider in the hanging wall than the footwall, but there is no apparent relationship between interval affected by drag and lithology. However, drag is less abundant at deeper stratigraphic levels where the sediments are more consolidated.
(6) To fully take advantage of dipmeter data, several different display methods should be used. The use of stereonet plots and cumulative dip and dip direction plots are especially valuable where much scatter of dip and azimuth measurements exists. If the data quality is good, the statistical curvature analysis technique of Bengtson (1981) is more appropriate. If very detailed analyses are needed, the normal 'tadpole' plots may be used after a thorough quality check of the raw data.

Acknowledgements

The authors want to thank Norsk Hydro, Saga Petroleum and Statoil for permission to publish these results. The article has benefited from extensive reviews by Roy Gabrielsen, Mike Badley and one anonymous referee. Assistance by Astri Rørnes, Margrethe M. Faaberg, Lars Aamodt, and Sidsel Haugland during the work is appreciated.

References

Adams, J. T., Ayodele, J. K., Bedford, J., Kaars-Sijpesteijn, C. H., & Watts, N. L. (1992). Application of dipmeter data in structural interpretation, Niger Delta. In A. Hurst, C. M. Griffiths and P. F. Worthington, (Eds.), *Geological Applications of Wireline Logs II*, (pp. 247–264) *Geological Society of London*, 65, *Special Publication*.

Badley, M. E., Price, J. D., Rambech Dahl, C., & Adestein, T. (1988). The structural evolution of the northern Viking Graben and its

bearing upon extensional modes of graben formation. *Geological Society of London*, *145*, 455–472.

Beach, A., Bird, T., & Gibbs, A. (1987). Extensional tectonics and crustal structure: deep seismic reflection data from the northern North Sea Viking Graben. In M. P. Coward, J. F. Dewey, and P. L. Hancock, (Eds.), *Continental extensional tectonics*, (pp. 467–476) *Geological Society*, *Special Publication*, 28.

Bengtson, C. A. (1981). Statistical curvature analysis techniques for structural interpretation of dipmeter data. *American Association of Petroleum Geologists Bulletin*, *65*, 312–332.

Bigelow, E. L. (1993). Multiwell dipmeter interpretation. *4th Annual SPE et al. Archie Conference Proceedings*, 73–80.

Devilliers, M. C., & Werner, P. (1990). Example of fault identification using dipmeter data. In A. Hurst, M. A. Lovell, and A. C. Morton, (Eds.), *Geological Applications of Wireline Logs*, (pp. 287–295). *Geological Society*, *Special Publication*, 48.

Dumont, A., Kubacsi, M., & Chardac, J. L. (1987). The oil-based mud dipmeter tool. *28th Annual SPWLA Logging Symposium*, *2*, 15 pp.

Etchecopar, A., & Bonnetain, J. L. (1989). Cross sections from dipmeter data. *American Association of Petroleum Geologists Bulletin*, *5*, 621–637.

Fossen, H., & Gabrielsen, R. H. (1996). Experimental modeling of extensional fault systems. *Journal of Structural Geology*, *18*, 673–687.

Fossen, H., & Hesthammer, J. (1998). Structural geology of the Gullfaks Field, northern North Sea. In M. P. Coward, H. Johnson, and T. S. Daltaban, (Eds.), *Structural geology in reservoir characterization*, *Geological Society of London*, *Special Publications*, 127 (pp. 231–261).

Fossen, H., Odinsen, T., Færseth, R. B., & Gabrielsen, R. H. (in press). Detachments and low-angle faults in the northern North Sea rift system. In A. Nøttvedt (Ed.), *Integrated Basin Studies*, *Geological Society of London*, *Special Publications*.

Fossen, H., & Rørnes, A. (1996). Properties of fault populations in the Gullfaks Field, northern North Sea. *Journal of Structural Geology*, *18*, 179–190.

Færseth, R. B. (1996). Interaction of Permo-Triassic and Jurassic extensional fault-blocks during the development of the northern North Sea. *Geological Society of London*, *153*, 931–944

Færseth, R. B., Sjøblom, T. S., Steel, R. J., Liljedahl, T., Sauar, B. E., & Tjelland, T. (1995). Tectonic controls on Bathonian-Volgian synrift successions on the Visund fault block, northern North Sea. In R. J. Steel et al., (Eds.), *Sequence stratigraphy on the Northwest European margin*, (pp. 325–346). *NPF Special Publication* 5.

Gabrielsen, R. H., Færseth, R. B., Steel, R. J., Idil, S., & Kløvjan, O. S. (1990). Architectural styles of basin fill in the northern Viking Graben. In D. J. Blundell, and A. D. Gibbs, (Eds.), *Tectonic evolution of the North Sea rifts*, (pp. 158–179). Clarendon Press, Oxford.

Gauthier, B. D., & Lake, S. D. (1993). Probabilistic modeling of faults below the limit of seismic resolution in Pelican Field, North Sea, offshore United Kingdom. *Bulletin American Association of Petroleum Geologists*, *77*, 761–777.

Giltner, J. P. (1987). Application of extensional models of the northern Viking Graben. *Norsk Geologisk Tidsskrift*, *67*, 339–352.

Goetz, J. F. (1988). Reliable dip data in oil based mud: Hardware and software considerations. *11th SPWLA Norwegian Chapter et al. Europe Formation Evaluation Symposium*, *Y*, 21 pp.

Goetz, J. F. (1994). A common sense approach to dipmeter interpretation. *Log Analyst*, *35*, 21–30.

Hesthammer, J. (1998a). Evaluation of the timedip, correlation and coherence map for structural interpretation of seismic data. *First Break*, *16*, 151–167.

Hesthammer, J. (in press, (b)) Integrated use of well data for structural control of seismic interpretation. *Petroleum Geoscience*, *4*, 97–109.

Hesthammer, J., & Fossen, H. (1997a). Seismic attribute analysis in structural interpretation of the Gullfaks Field, northern North Sea. *Petroleum Geoscience*, *3*, 13–26.

Hesthammer, J., & Fossen, H., (1997b). The influence of noise in structural interpretation of seismic data. *First Break*, *15*, 209–219.

Hesthammer, J., & Løkkebø, S. (1997). Combining seismic data sets to enhance data quality. *First Break*, *15*, 103–115

Hobbs, B. E., Means, W. D., & Williams P. F. (1976). An outline of structural geology. Wiley International, New York, 571 pp.

Hurley, N. F. (1994). Recognition of faults, unconformities, and sequence boundaries using cumulative dip plots. *American Association of Petroleum Geologists Bulletin*, *78*, 1173–1185.

Kaya, M. A., & Norman, T. N. (1993). Verifying a geological structure by applying SCAT (statistical curvature analysis techniques) method on dipmeter data at the Umurca Field in the Turkish Thrace. *4th Annual SPE et al. Archie Conference Proceedings*, 67–72.

Knipe, R. J. (1997). Juxtaposition and seal diagrams to help analyze fault seals in hydrocarbon reservoirs. *American Association of Petroleum Geologists*, *81*, 187–195.

Koepsell, R. J., Jenson, F. E., & Langley, R. L. (1989a). Formation imaging—1: Formation imaging yields precise fault orientation, minimizes dry offsets. *Oil & Gas Journal*, *87*, 55–58.

Koepsell, R. J., Jenson, F. E., & Langley, R. L. (1989b). Formation imaging—2: Imaging aids visualization of faults. *Oil & Gas Journal*, *87*, 85–86.

Needham, D. T., Yielding, G., & Freeman, B. (1996). Analysis of fault geometry and displacement patterns. In D. A. Nieuwland, and P. G. Buchanan, (Eds.), *Modern Development in Structural Interpretation*, *Validation and Modelling*, (pp. 189–199). *Geological Society of London*, *Special Publications*, *99*.

Roberts, A. M., Yielding, G., & Badley, M. E. (1990). A kinematic model for the orthogonal opening of the Late Jurassic North Sea rift system, Denmark-Mid Norway. In D. J. Blundell and A. D. Gibbs, (Eds.), *Tectonic evolution of the North Sea Rifts*, (pp. 180–199). Clarendon Press, Oxford.

Roberts, A. M., Yielding, G., Kusznir, N. J., Walker, I. M., & Dorn-Lopez, D. (1995). Quantitative analysis of Triassic extension in the northern Viking Graben. *Journal of Geological Society of London*, *152*, 15–26.

Rouby, D, Fossen, H., & Cobbold, P. R. (1996). Extension, displacement and block rotation in the larger Gullfaks area, northern North Sea: determined from map view restoration. *Bulletin American Association of Petroleum Geologists*, *80*, 875–890.

Rønningsland, T. M. (1990). Structural interpretation of dipmeter results in the Gullfaks Field. In A. Hurst, M. A. Lovell and A. C. Morton, (Eds.), *Geological Applications of Wireline Logs*, (pp. 273–286). *Geological Society of London Special Publication*, *48*.

Schlumberger (1986). Dipmeter interpretation. Schlumberger Limited, New York, 76 pp.

Schlumberger (1990). Data services catalog. Schlumberger Educational Services, Texas, 108 pp.

Schlumberger (1991). Wireline services catalog. Schlumberger Educational Services, Texas, 111 pp.

Scholz, C. H., Dawers, N. H., Yu, J.-J., Anders, M. H., & Cowie, P. A. (1993). Fault growth and fault scaling laws: preliminary results. *Journal of Geophysical Research*, *98*, 21951–21962.

Serra, O. (1989). Formation MicroScanner Image interpretation. Schlumberger Educational Services, Texas, 117 pp.

Stuart-Bruges, W. P. (1984). A dipmeter for use in oil based muds. *9th International SAID (division of SPWLA) Formation Evaluation Symposium*, 15 pp.

Thorne, J. A., & Watts, A. B. (1989). Quantitative analysis of North Sea subsidence. *American Association of Petroleum Geologists Bulletin*, *73*, 88–116.

Tollefsen, S., Graue, E., & Svinddal, S. (1994). Gullfaks development provides challenges: Pt. 1. *World Oil*, *215*, 45–54.

Trudgill, B., & Cartwright, J. (1994). Relay-ramp forms and normal-fault linkages, Canyonlands National Park, Utah. *American Association of Petroleum Geologists Bulletin*, *106*, 1143–1157.

Walsh, J. J., & Watterson, J. (1987). Distributions of cumulative displacement and seismic slip on a single normal fault surface. *Journal of Structural Geology*, *9*, 1039–1046.

Werner, P., Piazza, J. L., & Raiga-Clemenceau, J. (1987). Using dipmeter data for enhanced structural interpretation from the seismic. *28th Annual SPWLA Logging Symposium*, *2,* 15 pp.

Ziegler, P. A. (1982). Geological atlas of western and central Europe. Shell International Petrol., Maatshappij B. V.

Zhang, Y. (1993). Fault identification in Qiu Ling oilfield with diplog data. *Well Logging Technology*, *17*, 285–288.